



UNIVERSITY OF LEEDS

This is a repository copy of *Evaluation of combustion mechanisms using global uncertainty and sensitivity analyses: A case study for low-temperature dimethyl ether oxidation*.

White Rose Research Online URL for this paper:  
<http://eprints.whiterose.ac.uk/81505/>

Version: Accepted Version

---

**Article:**

Tomlin, AS, Agbro, E, Nevrlý, VC et al. (2 more authors) (2014) Evaluation of combustion mechanisms using global uncertainty and sensitivity analyses: A case study for low-temperature dimethyl ether oxidation. *International Journal of Chemical Kinetics*, 46 (11). 662 - 682. ISSN 0538-8066

<https://doi.org/10.1002/kin.20877>

---

**Reuse**

Unless indicated otherwise, fulltext items are protected by copyright with all rights reserved. The copyright exception in section 29 of the Copyright, Designs and Patents Act 1988 allows the making of a single copy solely for the purpose of non-commercial research or private study within the limits of fair dealing. The publisher or other rights-holder may allow further reproduction and re-use of this version - refer to the White Rose Research Online record for this item. Where records identify the publisher as the copyright holder, users can verify any specific terms of use on the publisher's website.

**Takedown**

If you consider content in White Rose Research Online to be in breach of UK law, please notify us by emailing [eprints@whiterose.ac.uk](mailto:eprints@whiterose.ac.uk) including the URL of the record and the reason for the withdrawal request.



[eprints@whiterose.ac.uk](mailto:eprints@whiterose.ac.uk)  
<https://eprints.whiterose.ac.uk/>

# Evaluation of combustion mechanisms using global uncertainty and sensitivity analyses: a case study for low temperature DME oxidation

---

Alison S. Tomlin<sup>1\*</sup>, Edirin Agbro<sup>1</sup>, Václav Nevrlý<sup>2</sup>, Jakub Dlabka<sup>2</sup>, Michal Vašínek<sup>3</sup>

<sup>1</sup>Energy Research Institute, University of Leeds, Leeds, UK, LS29JT

<sup>2</sup>VŠB-Technical University of Ostrava, Faculty of Safety Engineering, Ostrava, Czech Republic

<sup>3</sup>VŠB-Technical University of Ostrava, Faculty of Electrical Engineering and Computers Science, Ostrava, Czech Republic

\*Corresponding author: [A.S.Tomlin@leeds.ac.uk](mailto:A.S.Tomlin@leeds.ac.uk)

## Abstract

A global uncertainty analysis is performed for three current mechanisms describing the low temperature oxidation of dimethyl ether (Aramco Mech 1.3, Zheng et al. 2005, Liu et al. 2013) with application to simulations of species concentrations ( $\text{CH}_2$ ,  $\text{H}_2\text{O}_2$ ,  $\text{CH}_3\text{OCHO}$ ) corresponding to existing data from an atmospheric pressure flow reactor, and high pressure ignition delays. When incorporating uncertainties in reaction rates within a global sampling approach, the distributions of predicted targets can span several orders of magnitude. The experimental profiles however, fall within the predictive uncertainty limits. A variance based sensitivity analysis is then undertaken using high dimensional model representations. The main contributions to predictive uncertainties come from the  $\text{CH}_3\text{OCH}_2+\text{O}_2$  system, with isomerisation, propagation, chain-branching, secondary OH formation and peroxy-peroxy reactions all playing a role. The response surface describing the relationship between sampled reaction rates and predicted outputs is complex in all cases. Higher-order interactions between parameters contribute significantly to output variance, and no single reaction channel dominates for any of the conditions studied. Sensitivity scatter plots illustrate that many different parameter combinations could lead to good agreement with specific sets of experimental data. The Aramco scheme is then updated based on data from a recent study by Eskola et al. which presents quite different temperature and pressure dependencies for the rates of  $\text{CH}_3\text{OCH}_2\text{O}_2\rightarrow\text{CH}_2\text{OCH}_2\text{O}_2\text{H}$  and  $\text{CH}_2\text{OCH}_2\text{O}_2\text{H}\rightarrow\text{OH}+2\text{CH}_2\text{O}$  compared with currently used values, and includes well skipping channels. The updates from Eskola worsen the agreement with experiments when used in isolation. However, if the rate of the  $\text{CH}_2\text{OCH}_2\text{O}_2\text{H}+\text{O}_2$  channel is subsequently reduced, very good agreement can be achieved. Due to the complex nature of the response surface, the tuning of this channel remains speculative. Further detailed studies of the temperature and pressure dependence of the  $\text{CH}_3\text{OCH}_2\text{O}_2+\text{O}_2$ ,  $\text{CH}_2\text{OCH}_2\text{O}_2\text{H}+\text{O}_2$  system are recommended in order to reduce uncertainties within current DME mechanisms for low temperature conditions.

## 1. Introduction

Cleaner combustion devices based on the utilization of oxygenated fuels provide promising options for the development of lower carbon strategies in the transportation and energy sectors in the near future<sup>1</sup>. According to Fleisch et al., the high heating value, high cetane number and the ability of dimethyl ether (DME) to provide very low gaseous and particulate emissions makes it an ideal substitute for most existing direct injection diesel engines<sup>2</sup>. It is argued that NO<sub>x</sub> emissions using DME should be typically lower than when using diesel as a fuel since ignition delays are shorter<sup>1</sup>. The ability of combustion models to predict emission properties and ignition delays is therefore critical to designing practical combustion devices which may use this fuel optimally. The availability of accurate and

reliable detailed chemical kinetic models of DME oxidation is therefore of key importance for the further development of simplified schemes that could be used in the context of simulating practical combustion devices. Nevertheless, reducing uncertainties in predicted ignition characteristics and concentrations of minor products from the combustion of ethers or furans still remains a challenging task for combustion modellers. DME, being a simple candidate for an oxygenated fuel, provides a useful reference case for other oxygenated fuels in this context<sup>3</sup>.

Several DME oxidation mechanisms have been proposed in the literature that could potentially form the starting point for the development of reduced schemes<sup>4-7</sup>, but as is the case with many fuels, the mechanisms may display either mechanistic, or parametric differences. It is therefore useful to perform an evaluation of such mechanisms, to explore any major differences, and to evaluate how inherent uncertainties in their input data may impact on the predictive capability of the schemes with respect to available target experimental data. Liu et al. in particular, highlight the over-prediction of key intermediates HO<sub>2</sub> and H<sub>2</sub>O<sub>2</sub> by current schemes and suggest that currently available kinetic mechanisms of DME may contain large uncertainties at high pressure<sup>7</sup>. In the longer term, uncertainties in key parameters may be decreased by, for example, performing new kinetic studies. Assessing the sensitivity of selected predictive targets (e.g. species concentrations, ignition delays) to potential uncertainties within the input data to such schemes can be explored to assist this process<sup>8</sup> by helping to identify the most important reactions within a scheme, which determine the accuracy to which key combustion properties can be predicted. These parameters (e.g. rate constants etc.) can then be the subject of more detailed experimental and theoretical studies in order to provide their improved quantification, thus helping to improve the predictive accuracy and robustness of the schemes.

Whilst it is becoming increasingly common for individual studies of reaction mechanisms to provide a linear sensitivity analysis with respect to selected target predictions, assessments of the overall predictive uncertainties of mechanisms, given uncertainties in their input parameters, are less commonly addressed. One reason for this is that in order to investigate the influence of parametric uncertainty across wide regions of high dimensional input parameter space, computationally intensive sampling strategies are required. Monte Carlo random sampling approaches have previously been applied in this context but for systems with a large number of parameters (and most combustion mechanisms fall into this category), the number of runs required to achieve convergence of key statistics such as predicted target means and variance, can be very large. More recently, structured sampling approaches have been investigated for the purpose of uncertainty quantification and evaluation within combustions mechanisms with a recent study by Hébrard et al. demonstrating such an approach for low temperature butane oxidation<sup>9</sup>. A similar approach is adopted here, although in this study we do not restrict ourselves to a single mechanism, but rather try to compare the predictive uncertainty of several mechanisms and to explore the main causes of such uncertainty via a global sensitivity analysis related to the rate constants. Hence we perform a global uncertainty evaluation for three mechanisms describing the low temperature oxidation of DME which serves to highlight the main uncertainties and any differences between the schemes<sup>4-6</sup>. Selected experimental targets of interest include ignition delay times over a range of temperatures and pressures obtained from a rapid compression machine<sup>10</sup>, and intermediate species concentration data from an atmospheric pressure flow reactor operating at low temperatures (490-750 K)<sup>11</sup>.

## 2. Methodology

### 2.1. Kinetic Schemes

Three kinetic schemes representing the low temperature oxidation of DME are compared within this study. The first, hereby referred to as the “Liu2013” mechanism, is a recently updated version of the mechanism originally developed by Zhao et al<sup>4</sup> and consists of 295 reversible reactions and 55 species<sup>7</sup>. The main updates can be summarised as the replacement of the hydrogen subset by the model of Burke et al.<sup>12</sup>, the update of several rate constants of the pressure-dependent DME decomposition reaction as outlined in ref<sup>7</sup> and updates to the thermochemistry data from the thermodynamic database of Goos, Burcat, and Ruscic<sup>13</sup>. The second mechanism, referred to as the “LLNL” mechanism, was obtained from Lawrence Livermore National Laboratory (LLNL) and is outlined in Zheng et al.<sup>5</sup> It is a skeletally reduced mechanism based on the scheme originally described in Fischer et al.<sup>14</sup>, and contains 251 reversible reactions and 49 species. The third scheme is a comprehensive hierarchical scheme describing the oxidation

of small hydrocarbons and oxygenated fuels developed at NUI Galway<sup>6</sup>. It will be referred to here as the “Aramco” mechanism and consists of 766 reversible reactions and 125 species. In previous work, each of these schemes has been evaluated against experimental data sets as described in the papers referred to above. Having been developed as a more general scheme, the Aramco scheme in particular has been validated over a wide range of initial conditions and experimental devices, including flow reactor, shock tube, jet-stirred reactor, and flame studies for a range of starting fuels. However, a comprehensive comparison of these schemes in terms of their ability to predict low temperature DME oxidation, and the impact of choice of rate constant parameterisation and inherent uncertainties has not yet been performed and is a key aim of this study.

## 2.2. Flow Reactor Simulations

Flow reactor simulations were performed in order to investigate the ability of the mechanisms to predict the formation of key intermediate species. Based on the experimental data from Guo et al.<sup>11</sup>, the focus is on the target species CH<sub>2</sub>O, CH<sub>3</sub>OCHO and H<sub>2</sub>O<sub>2</sub>. Laminar flow reactor data were chosen for the purpose of our study, because they quantitatively describe the main features of DME low-temperature oxidation and also exhibit a reduced complexity of temperature profile compared to other recent studies such as Herrmann et al.<sup>15</sup>. In the context of a global sensitivity analysis using sampling based methods, the ability to utilise a simplified modelling strategy based on zero dimensional calculations in the spatial sense, makes the problem computationally tractable even when thousands of samples are required.

The Princeton laminar flow tube reactor has an inner diameter of 17 mm and an overall length of 355 mm. Within this study it was treated as a coupled pair of serially interconnected isothermal sub-reactors representing: (i) the initial nearly constant temperature part of the flow reactor; (ii) the end section of the flow reactor (approx. 100 mm) which exhibits a slight temperature decrease due to heat release near the exit. The central reactor temperature  $T_c$ , based on reported experimental data,<sup>11</sup> was assigned to the first sub-reactor. The value of  $T_c$  is taken to be representative for the simulation cases chosen for the current uncertainty study and this temperature is reported in the subsequent simulation results and uncertainty quantification. The temperature of the second sub-reactor  $T_m$  was set to be  $0.95T_c$  based on available experimental temperature profiles for central reactor temperatures of 613 K and 733 K. A fixed residence time of 1.7 s was chosen based on available experimental data. The pressure is 1 atmosphere and the cases selected for study here correspond to an equivalence ratio of  $\phi=0.6$ . The Cantera software libraries (version 2.0.2)<sup>16</sup> within the Python environment were employed for modelling the concentrations of target species in the laminar flow tube reactor as well as ignition delay times within the rapid compression machine (described within the next section).

Whilst the model represents a simplification of the experimental temperature profile, it enables us to perform the process of global sensitivity and uncertainty analysis in straightforward way, which given the sample sizes required makes the problem tractable. A time-step of  $\Delta\tau = 0.5$  ms was chosen, and suitable combinations of absolute and relative tolerances were used in order to achieve consistent convergence to steady-state. The predicted steady-state mole fractions of the target species CH<sub>2</sub>O, CH<sub>3</sub>OCHO, H<sub>2</sub>O<sub>2</sub> were chosen for subsequent uncertainty and sensitivity analyses. Under the assumptions described above, about 1 minute was required for each individual sample calculation on single core processor. According to Saltelli et al.<sup>17</sup>, this computational cost can be understood to be a reasonable upper limit for adopting the methods of variance based sensitivity analysis requiring several thousands of model runs.

## 2.3. Ignition Delay Simulations

In the experiments of Mittal et al.<sup>10</sup>, DME/O<sub>2</sub>/N<sub>2</sub> mixtures were investigated over a temperature range of 615-735 K, a pressure range of 10-20 bar, and equivalence ratios of 0.43 -1.5. Here numerical simulations were performed using Cantera for selected conditions covering this range of temperatures, pressures and equivalence ratios. Many studies assume that the effect of the compression process on predicted ignition delays is negligible. However, based on computational singular perturbation (CSP) analysis carried out by Mittal and co-workers<sup>10</sup> it was concluded that the compression stroke could greatly influence predicted ignition delay times due to the production of small radical pools during the compression stroke. The modelling approach adopted here is therefore in line with that of Mittal, in which both compression and post compression events are accounted for. The compression stroke is modelled by varying the volume of the simulated RCM reactor chamber with time. The volume history during compression is computed from

the geometric parameters (stroke, bore, acceleration time, deceleration time, total compression time etc.) of the RCM. The total time taken to complete the compression stroke is divided into three time stages given by:

$$t_{comp} = t_{accel} + t_{const} + t_{decel} \quad (1)$$

Where  $t_{comp}$  is the total time for compression,  $t_{accel}$  is the uniform acceleration time,  $t_{const}$  is the constant velocity time and  $t_{decel}$  is the uniform deceleration time.

Heat loss effects during and after compression, are accounted for by specifying an effective volume as a function of time. Details of the procedure can be found in Mittal and Sung<sup>18</sup>. In summary, the model which defines the volume of the RCM reactor chamber with heat loss effect taken into account is given by:

$$\text{while } t \leq t_{comp}: V(t) = V_g(t) + V_{add} \quad (2)$$

$$\text{while } t > t_{comp}: V(t) = V(t_{comp}) * V_p(t) \quad (3)$$

where  $V(t)$  is the time-dependent effective volume of the reactor chamber,  $V_g(t)$  is the geometric volume of the reactor chamber,  $V(t_{comp})$  is the volume at the end of compression and  $V_p(t)$  is the polynomial fit used to match the volume expansion trace  $V_{exp}(t)$  determined from the pressure trace of the non-reactive experiment.  $V_{add}$  is an empirical volume parameter that is added to the geometric volume of the reactor chamber at any time  $t$  in order to match the simulated pressure trace during the compression period with the experimental data. Based on assumption of adiabatic expansion,  $V_{exp}(t)$  is given by:

$$V_{exp}(t) = \left( \frac{P(0)}{P(t)} \right)^{1/\gamma} \quad t \geq 0 \quad (4)$$

where  $P(0)$  is the initial pressure and  $\gamma$  the specific heat ratio. The geometric parameters of the RCM and the empirical effective volume parameters (or heat loss parameters) used in modelling these specific experiment are available from the University of Connecticut combustion diagnostics laboratory experimental database<sup>19</sup>. Appropriate tolerance criteria were chosen to ensure sufficiently stable and well converged solutions across the three selected kinetic schemes.

#### 2.4. Uncertainty and Sensitivity Analysis Methods

A key aim of the study is to investigate the robustness of the mechanisms by estimating predictive error bars based on uncertainties within the model parameterisation. This can provide information on the appropriateness of the model structure, since if there are large deviations between experimental data and model data when taking into account error bars, then it may suggest missing model components e.g. reaction steps, physical processes etc. In addition, the error bars can indicate under which conditions uncertainties within the mechanisms lead to significant predictive uncertainties. For example, a recent uncertainty quantification of a butane oxidation scheme indicated larger predictive uncertainty within the negative temperature coefficient (NTC) temperature region compared to lower and higher temperatures<sup>9</sup>. A further aim of the study is to decompose the predictive uncertainty, in this case represented by the predicted output variance, in terms of the relative contributions from input uncertainties. Classical approaches to such variance based sensitivity analysis can require a large number of model runs, since a sampling approach has to be adopted in order to ensure that all sensitive regions of the input space are covered. Using Monte Carlo integrals for example requires  $N(2m+2)$  runs where  $N$  is the sample size chosen to represent the integrals, and  $m$  is the number of parameters<sup>20</sup>. For systems with a large number of parameters a two stage process is often used, where a screening of parameters is first carried out using a simple sensitivity method such as a brute force linear approach<sup>21,22</sup> or correlation methods<sup>9</sup>. The insensitive parameters are then excluded from subsequent global sampling based methods. For large mechanisms studied in combustion, the number of parameters excluded at this stage is usually large, with typically less than 50 being taken forward to the global analysis<sup>9,21,22</sup>. Further computational savings can then be achieved by adopting surrogate modelling approaches for the variance decomposition. Such methods are further discussed below.

The freely available C++ kernel of the Cantera toolbox was interfaced via specific-purpose Python scripts designed to automatically perform appropriate calculations within the individual stages of the sensitivity study. In all cases we focus on rate constants for the purposes of the uncertainty quantification. For the Liu2013 and Aramco schemes, only the forward rates are modified within the uncertainty study. For the LLNL scheme, the irreversible skeletal form of the scheme is chosen and both rates are modified separately within the uncertainty evaluation, thus allowing an investigation of potentially important thermochemistry from the analysis of the relative importance of forward vs. reverse steps. At the first stage, a screening analysis based on linear sensitivity methods was applied over the various conditions (P,T, $\phi$ ) chosen for the analysis. A subset of reactions was then selected according to the screening to carry forward to the global sensitivity and uncertainty study. Each stage of this process will now be described in more detail.

#### 2.4.1. Linear screening method

If all parameters were retained for the global sensitivity analysis then the dimension of the sample space would be very large, over 700 in the case of the full Aramco scheme. This makes for sparse samples unless very large sample sizes are used. It is therefore important to screen out unimportant reactions prior to the global sensitivity analysis in order to reduce the sparsity of the sample used for fitting the global sensitivity coefficients. In reality uncertainties within a quite small fraction of the total number of rate constants will determine the output uncertainty and the simulations are likely to be insensitive to a large number of others. Several approaches for screening are commonly used. Here, a brute force linear sensitivity approach was applied. Each rate constant was increased by 25% in turn from its nominal value within each mechanism and the target concentrations or ignition delays were recalculated. In this way, only one simulation run is sufficient for each reaction including those with complex pressure dependant forms. For the flow reactor simulations the linear screening was performed for the reactor conditions of atmospheric pressure over temperatures between 550 K and 700 K for the three target species at 50 K intervals. For the RCM simulations, a range of temperatures, pressures and equivalence ratios spanning the conditions from the study of Mittal et al.<sup>10</sup>, were chosen (temperatures between 615 and 725K, pressures of 10 to 20 bar and  $\phi = 0.43-1.5$ ). In each case, if the perturbation caused greater than a 2% change in the predicted target quantity then the reaction was selected for inclusion within the subsequent global sensitivity/uncertainty study. Table 1 indicates the reactions selected by the screening for the cases included. In reversible form there are 50 in total, indicating that a fairly conservative threshold was chosen. An automatic optimisation method used within the global sensitivity analysis will further exclude any minor effects (see next section). The main notable differences between the reactions screened from the RCM simulations compared to the flow reactor species mole fraction simulations is the inclusion of reactions involving CH<sub>3</sub> in the case of ignition delays. Otherwise a similar group of reactions has been screened for each of the two data sets.

#### 2.4.2. Uncertainty quantification and global sensitivity analysis

The uncertainty quantification within this study is based on a global sampling approach. Within such an approach, the uncertainties within the inputs are represented by a given distribution (uniform, log-normal etc.), which is then sampled and propagated through the model, providing distributions of the final model predictions. What this means is that a large number of model runs are performed, each one representing a possible set of input parameter values from within their defined uncertainties, and a probability distribution function is generated from the set of predicted outputs. A substantial number of model runs may be required in order to obtain stable output statistics, such as the mean and variance of the predicted targets. The sampling approach used is critical, since we would like to obtain stable statistics using the lowest possible number of model runs in order to minimize overall computational costs. Once stable output distributions are obtained, error bars may be calculated using variance based measures (e.g.  $1\sigma$  or  $2\sigma$  errors) or percentile plots.

The first step of a global uncertainty/sensitivity study is to define uncertainty factors for the input parameters under investigation. Reactions that have been well studied over a number of years may be included within a data evaluation such as those of Baulch et al.<sup>23-25</sup> and Tsang et al.<sup>26,27</sup>. In such evaluations uncertainties in  $\log(k)$  are usually given and indicate distributions which are log-normal and centred around the recommended or nominal value. The uncertainty parameter  $f$  can be defined as:

$$f = \log_{10} \left( \frac{k^0}{k^{\min}} \right) = \log_{10} \left( \frac{k^{\max}}{k^0} \right) \quad (5)$$

where  $k^0$  is the recommended (most probable or nominal) value of the rate coefficient based on an assessment of available experimental and theoretical studies, and  $k^{\max}$  and  $k^{\min}$  are the extreme upper and lower, but still possible values. Rearranging this equation yields:

$$\frac{k^{\max}}{k^0} = 10^f \quad (6)$$

meaning that the rate coefficient  $k^0$  is uncertain according to a multiplication factor  $G = 10^f$  and on a logarithmic scale the upper and lower values are positioned symmetrically around the recommended value.

Uncertainty factors for each reaction rate have been obtained from data evaluations where available within this study. The uncertainty factors  $G_i$  for each reaction  $i$  are shown in Table 1. In many cases there were no evaluations available for the selected rate constants. In such cases uncertainty factors had to be estimated and the NIST data base was used for this purpose. The suggested uncertainties reflect the spread of recent data available for a reaction rate constant from NIST if several studies were present. If only a single experimental or theoretical study was found, or a rate constant was estimated, then an uncertainty factor of 10 was assumed. It is recognised that in many cases due to the lack of data evaluation, these  $G_i$  factors represent a best guess rather than being fully quantified. However, recent studies suggest that even high level theory calculations can lead to uncertainties of up to a factor of 10 for complex reactions with multiple transition states<sup>28</sup>. A factor of 10 therefore seems to be a reasonable upper limit for non-evaluated or estimated reactions where no detailed experimental kinetic studies have been performed within the relevant temperature ranges.

For pressure dependant reactions uncertainty factors were included for A-factors for both low and high pressure limits where available in the case of fall-off reactions. Otherwise  $G_i(A_c)$  was set to be equal to  $G_i(A_0)$ . For the Aramco mechanism, the PLOG formulation is used to represent pressure dependency within the reaction rates. In this case the same uncertainty factor was assigned to A-factors for all pressures defined in the mechanism since no other information was available.

The  $G_i$  factors were then used to create a quasi-random sample for the uncertainty quantification using a Sobol low discrepancy sequence<sup>29,30</sup>. A quasi-random sample is chosen over a standard Monte Carlo random sample since a number of studies, including several in combustion, have shown that quasi-random sequences exhibit better convergence properties<sup>21,31,32</sup>. Hence, the mean and standard deviation of the predicted output mean and variance will reach convergence within a lower number of model runs compared to using a standard Monte Carlo approach. The Sobol sequence creates a quasi-random set of numbers between 0 and 1 for the number of parameters under investigation over the chosen sample size  $N$  (where  $N$  varies between 256 and 8192 in this study) and is then used to create a sample which is uniform in  $\log(k_i)$  based on the  $G_i$  factors. Hence the upper limit for the rate constant will be  $G_i \times k_i$  and the lower limit  $k_i/G_i$  and we sample uniformly between  $\log(k_i) - \log(G_i)$  and  $\log(k_i) + \log(G_i)$ . We use a uniform sample here since many of the  $G_i$  factors are not sourced from evaluated data and hence there is no real justification for using a probabilistic sampling approach such as a normal distribution.

As suggested above, classic Monte Carlo type approaches for a system with 50 varying parameters would lead to the requirement for extremely large sample sizes. The use of surrogate models for the calculation of sensitivity based indices helps to overcome this problem and several such methodologies have been developed and applied in combustion including those based on high dimensional model representations (HDMR)<sup>30,33,34</sup> and polynomial chaos expansions<sup>35,36</sup>. Both approaches are response surface methods (RSM) where a response surface approximation is first calculated which describes the relationship between the uncertain parameters in the original model and selected target outputs. The functional form of this approximation is then used to estimate the contribution of each parameter (or pairs of parameters etc.) to the overall variance of the predicted targets. The approximation is achieved by first running a

sample of full model simulations based on input parameter distributions as described above. A model approximation or meta-model is then constructed, which can be used as a surrogate for the full model in order to perform subsequent uncertainty and sensitivity analysis. The accuracy of the meta-model influences the accuracy of the calculated sensitivity indices and depends on various factors such as the sample size used, the fitting approach taken and the complexity of the response surface. High dimensionality of model input parameter space does not always imply a complex functional relationship between the more influential model inputs and target outputs and therefore accurate fits can often be achieved with an affordable number of model runs. The required sample size can be difficult to estimate, since it depends on the shape of the input-output response surface which is not known a-priori. However, experience shows that typically first-order sensitivities can be derived using ~1000 model runs<sup>9</sup>. If significant higher order effects are present due to parameter interactions, then significantly larger sample sizes may be needed<sup>20</sup>.

In the HDMR approach used here, a hierarchical expansion of the functional relationship between the inputs and outputs of a model is developed<sup>33,37</sup> using a response surface approximation based on orthonormal polynomials of the quasi-random sample of inputs  $x_i$ <sup>30</sup>. The expansion is expressed as the hierarchical sum of component functions of increasing order and is usually restricted to up to 2<sup>nd</sup> order terms:

$$f(\mathbf{x}) = f_0 + \sum_{i=1}^m f_i(x_i) + \sum_{1 \leq i < j \leq m} f_{ij}(x_i, x_j) + \dots + f_{12\dots m}(x_1, x_2, \dots, x_m) \quad (7)$$

Here the zero'th order component  $f_0$  denotes the mean value of the model response across the adopted sample. The first-order component functions  $f_i(x_i)$  give the effect of input  $x_i$  acting independently (although generally nonlinearly) upon the output  $Y(\mathbf{x})$ , and the function  $f_{ij}(x_i, x_j)$  is a second-order term describing the cooperative effects of the variables  $x_i$  and  $x_j$  upon the output  $Y(\mathbf{x})$ . This provides the ANOVA (Analysis Of Variances) decomposition of  $Y(\mathbf{x})$  as first discussed by Sobol', and therefore each term represents the relative influence of single parameters or pairs of parameters on the overall output variance<sup>38</sup>. The HDMR expansion is always of finite order<sup>39</sup> making it computationally efficient if higher-order input variable interactions are weak and can be neglected.

To reduce the sampling effort in HDMR, the higher-order component functions are approximated by expansions in terms of suitable basis functions which may include polynomials, splines etc. For example, expansion in terms of orthonormal polynomials is given by:

$$f_i(x_i) \approx \sum_{r=1}^k \alpha_r^i \varphi_r(x_i) \quad (8)$$

$$f_{ij}(x_i, x_j) \approx \sum_{p=1}^l \sum_{q=1}^{l'} \beta_{pq}^{ij} \varphi_p(x_i) \varphi_q(x_j)$$

...

where  $k, l, l'$  represent the order of the polynomial expansion,  $\alpha_r^i$  and  $\beta_{pq}^{ij}$  are constant coefficients to be determined, and  $\varphi_r(x_i)$ ,  $\varphi_p(x_i)$  and  $\varphi_q(x_j)$  are the orthonormal basis functions, which in the current study are based on shifted Legendre polynomials of up to 6<sup>th</sup> order. The coefficients are determined using Monte Carlo integration over the chosen input sample<sup>40</sup>. The approximation of the component functions reduces the sampling effort dramatically so that only one set of quasi-random samples  $N$  is necessary in order to determine all RS-HDMR component functions and subsequently the sensitivity indices. A slightly different approach is adopted in polynomial chaos methods where the uncertainties in inputs are first expressed as polynomial expansions of random basis variables and the model outputs are then expressed as (usually low-order) functions of these random inputs<sup>41</sup>. For practical applications, if similar orders of expansion and polynomial expressions are used, then the response surface approximation should not differ greatly between the methods.

Based on equation (8) the partial variances  $D_i, D_{ij}, \dots$  for sensitivity analysis purposes are obtained from:

$$D_i \approx \sum_{r=1}^{k_i} (\alpha_r^i)^2 \quad (9)$$

$$D_{ij} \approx \sum_{p=1}^{l_i} \sum_{q=1}^{l_j} (\beta_{pq}^{ij})^2 \quad (10)$$

...

Normalising the partial variances by the overall variance  $D$  of  $f(\mathbf{x})$  gives the fractional contribution to the variance of each parameter or the sensitivity indices:

$$S_{i_1, \dots, i_s} = \frac{D_{i_1, \dots, i_s}}{D}, \quad 1 \leq i_1 < \dots < i_s \leq n. \quad (11)$$

First-order ( $S_i$ ) and second-order ( $S_{i,j}$ ) global sensitivity indices have been calculated in this work. If the output variance is fully described by the second-order HDMR meta-model then the sum of all  $S_i$  and  $S_{i,j}$ 's will be 1. Each individual sensitivity index describes the fraction of the output variance that is caused by the uncertainty in input parameter  $x_i$  or by uncertainty in pairs of parameters  $x_i$  and  $x_j$  acting cooperatively in the case of second-order indices. In most previous studies of kinetic systems, terms of third-order and higher have been found to be small. Further details on the method can be found in refs<sup>21,22,30,31</sup>.

### 3. Results

#### 3.1. Comparison with Experiment and Uncertainty Quantification

##### 3.1.1. Flow reactor studies

Figure 1 presents a comparison between the experimental species mole fraction profiles from the flow reactor, and simulations using the three mechanisms. In addition to the single profiles from the three base mechanisms, output distributions are shown reflecting the impact of input uncertainties. The solid lines represent the experimentally measured profiles, and the dashed lines show the profiles using the original parameters within each mechanism. Experimental errors were reported<sup>11</sup> for  $\text{H}_2\text{O}_2$  and are represented by the shaded region in Fig. 1c. For each of the three mechanisms, there is an over prediction of  $\text{H}_2\text{O}_2$  which is consistent with the previous findings of Liu et al.<sup>7</sup>. There are also significant discrepancies for formaldehyde and methyl formate predictions which span the temperature range. Each of the three mechanisms produce similar profiles although there are some differences between the predictive uncertainty which suggests some differences in the parameterisation of the main rate constants. Using the original parameterisations within the mechanisms, each has a tendency to under-predict  $\text{CH}_2\text{O}$  for temperatures up to 675 K. For  $\text{CH}_3\text{OCHO}$  there is a slight shift in the predicted peak with respect to temperature when compared to the experimental profile. Whilst this may be due to differences within the physical modelling (e.g. not using a 2-D model as suggested in Guo et al.<sup>11</sup>), the over prediction of the peak value is consistent with previous studies.

The box and whisker plots represent the region of uncertainty from the model predictions taking account of the input uncertainties specified in Table 1. A quasi-random sample of size  $N = 256$  was used for this purpose since mean and variance properties of the output distributions had converged by this point. The box and whiskers represent 25<sup>th</sup> and 75<sup>th</sup> percentiles respectively. The figure illustrates that the experimental profiles fall well within the limits of uncertainty as expressed by the 75<sup>th</sup> percentiles (upper quartile, whiskers) from the predicted output distributions for  $\text{H}_2\text{O}_2$  and  $\text{CH}_3\text{OCHO}$ . However, it should be noted that, particularly at low temperatures, the uncertainty can span several orders of magnitude. For predictions of  $\text{CH}_2\text{O}$  the experimental profiles for the low temperature region are in closest agreement with the upper quartiles from the predicted distributions suggesting that some important input parameters may need to be close to the edges of their input uncertainty ranges in order to reduce discrepancies. In the following section the causes of predictive uncertainties are explored via global sensitivity analysis and the main reactions contributing to variance are identified.

### 3.1.2. Ignition delay studies

Figure 2 presents a straightforward comparison between predicted ignition delays from each mechanism and experimental data provided by Mittal et al.<sup>10</sup>. There is reasonable agreement across much of the temperature range for all the schemes but also discrepancies which can reach a factor of 5 for the rich case of  $\phi = 1.5$ , 10 bar at higher temperatures. In Fig. 3 we show a similar uncertainty propagation to that shown in Fig. 1, focussing on predicted ignition delays for the case of  $\phi = 0.75$ , 10 bar. Whilst the predictions from the mechanisms based on their original parameterisation seem in reasonable agreement with the experimental data, the bounds of uncertainty are large, again spanning up to three orders of magnitude in some cases. This may at first appear to be counter intuitive. However, in the absence of detailed kinetic studies it seems likely that the parameterisation of some important reactions within the scheme have been informed by available experimental data such as ignition delays. In order to accurately predict ignition delays, the ratio of propagation to branching fluxes should be correct. Within the uncertainty analysis however, we have allowed each rate constant to vary independently, potentially shifting this balance, since any correlations are not explicitly represented within the mechanism parameterisations. We return to this point in the following discussion. It is also worth noting that the original parameterisations lead to significant discrepancies for species mole fractions within the flow reactor simulations. Hence it is of interest to explore whether a common set of reactions determine the output variance for both sets of target data since clearly the current parameterisations do not give good agreement in both cases.

## 3.2. Global Sensitivity Analysis

### 3.2.1. Flow reactor studies

Figure 4 shows the main first- and second-order sensitivity indices from the HDMR analysis of the flow reactor simulations with the shading for each reaction or pairs of reactions shown in the legend. 4096 simulations have been used within the HDMR approach in order to estimate sensitivity coefficients up to second-order. We restrict the results to the main 15 reactions that contribute to the output variance since this simplifies the discussion somewhat. The figure shows that these 15 reactions account for between 60-85% of the predictive variance across all mechanisms and temperatures studied, and hence are dominant in terms of their contributions to predictive uncertainties. It is clear from the figure that there are strong similarities between the sensitivity indices for each mechanism but there are also differences caused by differences in product channels or rate constant parameterisations between the schemes.

The critical pathways which dominate the uncertainty at low temperatures are shown in Fig. 5. These are a subset of those highlighted in the flux path analysis of Guo et al.<sup>11</sup> and hence not all the pathways which have strong fluxes contribute strongly to the predictive uncertainty within the mechanisms for the chosen targets. At 550 K the isomerisation reaction  $\text{RO}_2 = \text{QOOH}$  accounts for around 40% of the predictive uncertainty for each species mole fraction. For the LLNL scheme both forward and reverse channels were assessed separately and whilst there is some sensitivity to the reverse  $\text{QOOH} \rightarrow \text{RO}_2$ , indicating the importance of the enthalpy of formation of the QOOH species, the forward rate dominates. This suggests that the low temperature measurements of key intermediates such as those in the work of Guo et al.<sup>11</sup> could provide useful constraints on the forward reaction rate for the isomerisation of  $\text{RO}_2$  at low temperatures. This was the only reaction where significant sensitivity to the reverse rate was found within the LLNL scheme.

The first-order sensitivity with respect to  $\text{CH}_2\text{O}$  for this isomerisation reaction as indicated by the component function is positive over the majority of the parameter range at 550 K as shown in Fig. 6a. In each of the component function plots, the current nominal values within the mechanisms would be represented by a value of 0.5 on the x-axis (i.e. the mid-point within the uncertainty range). The solid line in the figure represents the individual response to changes in the rate of reaction for  $\text{RO}_2 = \text{QOOH}$  based on the Aramco scheme (i.e. the first-order HDMR component function based on equation 7), and the scatter indicates the additional uncertainty stemming from uncertainties within the other parameters within the scheme. Whilst a strong response is observed at the lower half of the chosen range for this rate constant, the effect saturates at higher values. However, since the experimentally measured mole fraction for  $\text{CH}_2\text{O}$  is about  $1 \times 10^{-3}$  the figure suggests that the rate of this reaction would need to be in the upper half of the input range in order for the simulations to overlap with experiment at this low temperature. As the rate of the isomerisation step increases we might expect to see sensitivities dominated by subsequent channels such as the competition between

chain branching and propagation. The first-order sensitivity with respect to methyl formate mole fraction for  $\text{RO}_2=\text{QOOH}$  at 550K is shown in Fig. 6b and displays an interesting nonlinearity. The response is positive at the lower end of the input range and negative at the higher. A large increase in this rate constant could therefore potentially reduce predicted  $\text{CH}_3\text{OCHO}$  but the impact on predicted  $\text{CH}_2\text{O}$  would depend on a number of other factors as suggested by the scatter in Fig. 6a at larger reaction rates. A fuller discussion of recent data for this reaction is given later.

The nonlinearity in response to changes in the isomerisation step highlights the need to calculate sensitivities right across the range of uncertainty rather than just at the nominal value. In addition, despite this reaction having the highest sensitivity index in some cases, there is a large amount of scatter in the response to changes in the rate constant, suggesting that several other reactions also play a role. The production of  $\text{CH}_2\text{O}$  is also particularly sensitive to the rates of the branching path  $\text{QOOH}+\text{O}_2$  vs. the propagation path  $\text{QOOH}=\text{OH}+2\text{CH}_2\text{O}$  which is consistent with the flux path analysis performed by Guo et al.<sup>11</sup> and the linear sensitivity analysis performed by Dagaut et al.<sup>42</sup>. There are also a number of important second-order effects of which the major one is between the isomerisation step and the  $\text{RO}_2+\text{RO}_2$  channel (see Fig. 4).

The isomerisation pathway  $\text{RO}_2=\text{QOOH}$  is the dominant reaction for uncertainties within predictions of methyl formate across all temperatures studied, and hence constraints on the temperature dependence of the reaction rate could be obtained from the temperature dependent methyl formate measurements. Interestingly, the shape and sign of the response to changes in this reaction rate with respect to methyl formate concentrations changes between 550 K and 650 K as shown by comparing Fig. 6b with Fig. 7a. Increasing the rate of the isomerisation pathway would reduce the production of methyl formate across most of the temperature range. The decomposition of  $\text{HO}_2\text{CH}_2\text{OCHO}$  is also particularly important for the formation of methyl formate and  $\text{H}_2\text{O}_2$  at low temperatures (see Fig. 4).

$\text{RO}_2+\text{RO}_2$  is also an important pathway at low temperatures, contributing around 15% of the uncertainty in  $\text{H}_2\text{O}_2$  predictions in the case of the Aramco mechanism and around 10% for  $\text{CH}_2\text{O}$ . The dominant product channels differ here between the schemes, with the Liu2013 mechanism showing a greater sensitivity to the formation of  $\text{CH}_3\text{OCH}_2\text{OH}$  compared to  $\text{CH}_3\text{OCH}_2\text{O}$  for the other schemes.

At higher temperatures, the prediction of  $\text{CH}_2\text{O}$  and  $\text{H}_2\text{O}_2$  become relatively insensitive to  $\text{RO}_2=\text{QOOH}$  and far more sensitive to the addition of  $\text{O}_2$  to  $\text{QOOH}$  and to the decomposition of  $\text{QOOH}$  to form  $\text{OH}$  and  $\text{CH}_2\text{O}$ . Above 650 K, over 40% of the variance in predicted  $\text{H}_2\text{O}_2$  is due to uncertainties in the rate of second  $\text{O}_2$  addition (see Fig. 4). The response is strongly non-linear across the range (Fig. 7b) with a high sensitivity at lower values for the rate constant, which begins to saturate at high values. This suggests that to reduce predicted  $\text{H}_2\text{O}_2$  concentrations to be more in line with experiments, the rate would have to be lower than the nominal values in the current mechanisms, although the data is quite scattered. The shape of the response of  $\text{CH}_2\text{O}$  for this reaction is the opposite of that for  $\text{H}_2\text{O}_2$  (Fig. 7c) which is consistent with an over prediction of  $\text{H}_2\text{O}_2$  and an under prediction of  $\text{CH}_2\text{O}$  with the mechanisms in their current form. However, whilst this reaction dominates uncertainties in predicted  $\text{CH}_2\text{O}$  between 600 K and 650 K, by 700 K the shape of its component function has changed, and at the lower end of the adopted uncertainty range it now exhibits a negative response (Fig. 7d). Hence overall a lowering of this rate would apparently increase  $\text{CH}_2\text{O}$  production at temperatures up to 650 K and would decrease it at 700 K. At 700 K the importance of reactions  $\text{DME} + \text{OH}$  and  $\text{CH}_2\text{O} + \text{OH}$  increases. At this temperature there are some critical differences between the mechanisms, with the Aramco and LLNL mechanisms showing higher sensitivity to the formation of  $\text{HOCH}_2\text{O}$  from  $\text{CH}_2\text{O} + \text{OH}$  and Liu2013 showing higher sensitivity to the formation of  $\text{HCO}$ .

### 3.2.2. Ignition delay studies

Figure 8 shows the main first- and second-order sensitivity indices from the HDMR analysis of selected ignition delay simulations with the shading for each reaction or pairs of reactions shown in the legend. 4096 simulations have been used for the LLNL and Liu2013 mechanisms and 8192 for the Aramco scheme within the HDMR approach, in order to estimate sensitivity indices up to second-order with a good accuracy for the main effects.  $P = 10$  bar for all simulations. Data where no ignition occurred or where the ignition occurred during the compression phase were removed from the fitting process. A boot-strapping method was used to check the convergence of the calculated indices.

The selected reactions are very consistent between the three mechanisms, with small variations in the relative size of the sensitivity indices. A smaller number of reactions are seen to play a role compared to the 15 shown for the flow reactor simulations in Fig. 4. However, it is also noticeable that a lower fraction of the overall variance can be accounted for using a second-order model for the higher temperature simulations. This may either be caused by the presence of effects which are higher than second-order, or the cumulative effect of very small second order terms which cannot be accurately captured without resorting to extremely large sample sizes.

For  $\phi = 0.75$  and  $T = 649$  K, the isomerisation reaction dominates with smaller contributions from the  $\text{CH}_2\text{OCH}_2\text{O}_2\text{H} + \text{O}_2 = \text{O}_2\text{CH}_2\text{OCH}_2\text{O}_2\text{H}$ ,  $\text{O}_2\text{CH}_2\text{OCH}_2\text{O}_2\text{H} = \text{HO}_2\text{CH}_2\text{OCHO} + \text{OH}$ , and  $\text{HO}_2\text{CH}_2\text{OCHO} = \text{OCH}_2\text{OCHO} + \text{OH}$  channels. The reactions of hydroperoxymethyl formate are therefore an important pathway for the formation of OH in the current form of all the mechanisms although Gao and Nakamura<sup>43</sup> question whether there are other possible secondary OH formation routes. At the higher temperatures, the competition between chain-propagation  $\text{QOOH} = \text{OH} + 2\text{CH}_2\text{O}$  and chain-branching  $\text{QOOH} + \text{O}_2$  increases in importance and the relative importance of the reactions of hydroperoxymethyl formate reduces. There are a number of important second-order terms although overall they do not contribute more than a few percent of the overall variance.

Figure 9 shows selected sensitivity plots for the predicted ignition delays at  $P = 10$  bar,  $\phi = 0.75$  and  $T = 703$  K, corresponding to the middle case in Fig. 8. Fig. 9a shows that whilst the overall first-order effect (solid line) is negative, as the isomerisation route gets faster, the spread in predicted ignition delays becomes much wider (up to 3 orders of magnitude). This type of behaviour is termed heteroscedasticity, and in the current case what this means is that the overall variance of the predicted ignition delays changes with the value of the selected rate constant for isomerisation. As the isomerisation becomes faster, increasing the rate of QOOH formation, then the competition between other reactions (e.g. branching vs. propagation) play an increasing role, and the range of predicted ignition delays broadens. The experimentally determined log of the ignition delay for these conditions is just over 1, and hence it is apparent that all of the 2 orders of magnitude span in the forward isomerisation rate constant could encompass the experimental data depending on the values of other rates.

The component function for the branching step  $\text{QOOH} + \text{O}_2$  is shown in Fig. 9b and unsurprisingly has a negative slope, indicating that slowing this rate will increase ignition delays. The individual first-order effect of changing this rate on ignition delays spans an order of magnitude based on the factor of 10 uncertainty which was assumed for this reaction. The equivalent component function for the propagation step (Fig. 9c), spans about a factor of 5. Data points lying far from the first-order effect (solid line) are usually indicative of higher-order terms where parameters will interact in their effects on predictive ignition delays. A strong second-order interaction exists between the branching and propagation channels and has a complex shape as shown in Fig 9d. Whilst this second-order term represents less than 3% of the overall variance, depending on parameter combinations, it can lead to order of magnitude changes in predicted ignition delays. These complex interactive effects can lead to wide predicted distributions and could make it difficult to tune data based on comparisons with experimental ignition delays as previously highlighted by Mittal et al.<sup>44</sup>. Whilst not shown, it is worth pointing out that the secondary OH production channel, from the decomposition of hydroperoxymethyl formate ( $\text{HO}_2\text{CH}_2\text{OCHO}$ ) has a response with a similar form to that of the  $\text{QOOH} + \text{O}_2$  step and is of equivalent importance at the lower temperature (649 K) but decreases in importance at higher temperatures.

#### 4. Discussion and Final Conclusions

The scatter within the sensitivity plots and the lack of dominance of any one reaction channel suggests that tuning rate constants in order to achieve a better fit to available experimental data sets is unlikely to lead to unique parameterisations. Whilst a full optimisation study, of the type performed by Turányi et al.<sup>45</sup>, would be possible for low temperature DME systems, it seems likely that large uncertainties may remain within optimised rate constants without the availability of further detailed kinetic studies of the main reaction channels. One such study has recently been performed by Eskola et al.<sup>46</sup>. Low temperature experimental data of the overall rate constant and OH yields and Master equation calculations were combined in order to provide temperature and pressure dependant rate constants for several reaction channels of importance to this study. In Fig. 10 we compare the estimated rate constants from their study with values currently used within the DME mechanisms for the forward rate of the isomerisation reaction  $\text{CH}_3\text{OCH}_2\text{O}_2 \rightarrow \text{CH}_2\text{OCH}_2\text{O}_2\text{H}$  (Fig. 10a) and the chain-propagation step  $\text{QOOH} \rightarrow \text{OH} + 2\text{CH}_2\text{O}$  (Fig. 10b). Based

on the Eskola study, both reactions show a pressure dependency that is not represented in the parameterisations used within the current mechanisms but has been suggested in previous work<sup>47</sup>. The suggested rate for the isomerisation step is significantly faster than the ones currently used over all temperatures and pressures. At lower temperatures the difference is greater than an order of magnitude. The apparent pressure dependence of the rate of the chain-propagation step from the study of Eskola et al.<sup>46</sup>, is not represented within current mechanisms, and the temperature dependence differs from that found by Eskola et al. The Eskola study also provides data for well skipping channels where the alkyl + O<sub>2</sub> step proceeds directly to RO<sub>2</sub>, QOOH or 2CH<sub>2</sub>O+OH and RO<sub>2</sub> directly forms 2CH<sub>2</sub>O+OH. A total of 9 pressure and temperature reaction rates are provided for the CH<sub>3</sub>OCH<sub>2</sub> + O<sub>2</sub> → CH<sub>3</sub>OCH<sub>2</sub>O<sub>2</sub> system by Eskola et al.<sup>46</sup> in the form of Chebyshev polynomials.

The impact of updating current rate constants using data from Eskola et al.<sup>46</sup>, and the addition of well skipping reactions on the current predictions was tested using the Aramco scheme for selected conditions. The updates for flow reactor simulations are shown as a grey dotted line in Fig. 1c. The agreement with experiment is worsened in almost all cases. The equivalent plot for predicted ignition delays at 10 bar and  $\phi = 0.75$  is shown in Fig. 3c. Again the agreement with experiment is worsened. However, it was noted within Fig. 9a that increasing the rate of the isomerisation channel led to greater scatter in the predicted ignition delays and an increase in importance of other reactions. As discussed above it is also likely that in the absence of detailed kinetic studies there are inevitably some inherent correlations within the current mechanisms based on tuning to available experimental data sets. Hence if only a subset of the important parameters are updated, then the balance between branching and propagation could be shifted leading to greater discrepancies with experiment and this needs to be compensated for. The low temperature updates to the rate of the propagation step were fairly small at 10 bar. Further changes to predicted ignition delays could be effected by modifications to the branching channels. This assumption was tested by making adjustments to the rate of QOOH + O<sub>2</sub>. We should stress that this is purely for illustration purposes and in general we would not recommend tuning rate constants based on limited comparisons with experiment. However, the effect of a reduction by a factor of 10 for this channel (in addition to the other updates) is illustrated for the flow reactor simulations at atmospheric pressure in Fig 1c by the dash-dotted line. The agreement with experiment is now much improved for each of the species with the peak in methyl formate concentration now occurring at the correct temperature. The equivalent update for the ignition delay data at 10 bar is shown in Fig 3c, except in this case a reduction in the rate constant by a factor of 5 gives very good agreement with the measured data. Since the two sets of data are at very different pressures, the slightly different levels of adjustment required may be indicative of a weak pressure dependency for the branching steps. This suggestion should be treated as speculative since previous studies have suggested only a weak pressure dependence for QOOH + O<sub>2</sub> in other systems compared to a strong pressure dependencies of the QOOH decomposition (propagation) channels<sup>48,49</sup>. However, considerable uncertainties also remain in the subsequent OH forming steps. The decomposition of hydroperoxymethyl formate (HO<sub>2</sub>CH<sub>2</sub>OCHO), which is formed in the first OH forming branching step, is of pronounced importance in this context. New mechanistic aspects related to the decomposition of HO<sub>2</sub>CH<sub>2</sub>OCHO have also been suggested based on theoretical calculations<sup>51</sup>. Reaction channels leading to formic acid (HCOOH) and the so-called Criegee intermediate (CH<sub>2</sub>OO) were concluded to be of comparable importance to O-O bond scission, which is assumed to be the unique channel for hydroperoxymethyl formate decomposition in current chemical kinetic schemes<sup>47</sup>. Assessment of the appropriateness and possible impact of implementing other reaction channels is beyond the scope of this study but it is clear that detailed studies of the pressure and temperature dependence of these reactions are required in order to improve agreement with available experimental targets and to reduce the overall uncertainties within predictions of low temperature DME oxidation.

Overall, the study has shown that uncertainties in predicting key target quantities for the low temperature oxidation of DME are currently large. These uncertainties however, are driven by a few key reactions within the schemes studied. Currently these reactions are based on very similar parameterisations within the schemes studied and only minor reaction channels appear to differ greatly between the three mechanisms tested. Sensitivity scatter plots, illustrating the response of the target quantities to changes in rate constants within a global uncertainty analysis, indicate the difficulties in tuning individual rate parameters to particular data sets. No single reaction dominates the uncertainty under any conditions and higher-order interactions can lead to large variance within predicted quantities. New data for the isomerisation and propagation steps highlight a pressure dependence for these channels that is not represented within currently used parameterisations. However, updates to the Aramco scheme based on this recently available data

when applied in isolation, worsen the overall agreement with experimental targets. The current lack of representation of the pressure dependence of key reactions may be one contributory reason why good agreement can be obtained between current mechanisms and experimental targets under some conditions (e.g. high pressure ignition delays), and not under others (e.g. over or under prediction of key minor products at atmospheric pressure). The study highlights the need for detailed pressure dependant studies of the chain branching steps:  $\text{CH}_2\text{OCH}_2\text{O}_2\text{H} + \text{O}_2 = \text{O}_2\text{CH}_2\text{OCH}_2\text{O}_2\text{H}$  and subsequent OH forming channels or competitive pathways, which are likely to dominate the remaining uncertainty if the isomerisation route is faster than currently assumed as suggested by recent updates to this rate constant.

## Acknowledgements

The authors would like to thank Robin Shannon, Mark Blitz, Paul Seakins, Struan Robertson and Mike Pilling for providing rate constant data for the isomerisation and propagation pathways and for helpful discussions. We thank the European Cost Action CM0901 for supporting scientific exchange visits and the Tertiary Education Trust Fund (TETFUND), Nigeria for scholarship funding for E. Agbro. The work was also supported by the Ministry of Education, Youth and Sports of the Czech Republic via projects LD11012 and LD12020.

## Bibliography

1. Arcoumanis, C.; Bae, C.; Crookes, R.; Kinoshita, E. *Fuel* 2008, 87, 1014-1030.
2. Fleisch, T.; McCarthy, C.; Basu, A.; Udovich, C.; Charbonneau, P.; Slodowska, W.; Mikkelsen, S.-E.; McCandless, J.; SAE International, 1995.
3. Kaiser, E. W.; Wailington, T. J.; Hurley, M. D.; Platz, J.; Curran, H. J.; Pitz, W. J.; Westbrook, C. K. *J Phys Chem A* 2000, 104, 8194-8206.
4. Zhao, Z.; Chaos, M.; Kazakov, A.; Dryer, F. L. *Int J Chem Kinet* 2008, 40, 1-18.
5. Zheng, X. L.; Lu, T. F.; Law, C. K.; Westbrook, C. K.; Curran, H. J. *Proc Combust Inst* 2005, 30, 1101-1109.
6. Metcalfe, W. K.; Burke, S. M.; Ahmed, S. S.; Curran, H. J. *Int J Chem Kinet* 2013, 45, 638-675.
7. Liu, D.; Santner, J.; Togbe, C.; Felsmann, D.; Koppmann, J.; Lackner, A.; Yang, X. L.; Shen, X. B.; Ju, Y. G.; Kohse-Hoinghaus, K. *Combust Flame* 2013, 160, 2654-2668.
8. Tomlin, A. S. *Proc Combust Inst* 2013, 34, 159-176.
9. Hebrard E; A.S. Tomlin; R. Bounaceura; Battin-Leclerc, F. *Proc Combust Inst* 2014, In press, 10.1016/j.proci.2014.06.027
10. Mittal, G.; Chaos, M.; Sung, C. J.; Dryer, F. L. *Fuel Process Technol* 2008, 89, 1244-1254.
11. Guo, H. J.; Sun, W. T.; Haas, F. M.; Farouk, T.; Dryer, F. L.; Ju, Y. G. *Proc Combust Inst* 2013, 34, 573-581.
12. Burke, M. P.; Chaos, M.; Ju, Y.; Dryer, F. L.; Klippenstein, S. J. *Int J Chem Kinet* 2012, 44, 444-474.
13. Goos, E.; Burcat, A.; Ruscic, B. *Extended Third Millennium Thermodynamic Database for Combustion and Air-Pollution Use.* : <http://garfield.chem.elte.hu/Burcat/BURCAT.THR>, 2013.
14. Fischer, S. L.; Dryer, F. L.; Curran, H. J. *Int J Chem Kinet* 2000, 32, 713-740.
15. Herrmann, F.; Jochim, B.; Oswald, P.; Cai, L. M.; Pitsch, H.; Kohse-Hoinghaus, K. *Combust Flame* 2014, 161, 384-397.
16. Goodwin, D. M., N; Moffat, H; Speth, R. <https://code.google.com/p/cantera>, 2013.
17. Saltelli, A.; Ratto, M.; Tarantola, S.; Campolongo, F. *Chem Reviews* 2005, 105, 2811-2828.
18. Mittal, G.; Sung, C.J. *Combust Sci Technol* 2007, 179, 497-530.
19. Sung, C. J. *The Combustion Diagnostics Laboratory Experimental Database:* <http://combdialab.engr.uconn.edu/database>, 2014.
20. Saltelli, A. *Comput Phys Commun* 2002, 145, 280-297.
21. Ziehn, T.; Hughes, K. J.; Griffiths, J. F.; Porter, R.; Tomlin, A. S. *Combust Theor Model* 2009, 13, 589-605.
22. Ziehn, T.; Tomlin, A. S. *Int J Chem Kinet* 2008, 40, 742-753.
23. Baulch, D. L.; Bowman, C. T.; Cobos, C. J.; Cox, R. A.; Just, T.; Kerr, J. A.; Pilling, M. J.; Stocker, D.; Troe, J.; Tsang, W.; Walker, R. W.; Warnatz, J. *J Phys Chem Ref Data* 2005, 34, 757-1397.
24. Baulch, D. L.; Cobos, C. J.; Cox, R. A.; Frank, J. H.; Hayman, G.; Just, T. H.; Kerr, J. A.; Murrels, T.; Pilling, M. J.; Troe, J.; Walker, B. F.; Warnatz, J. *Combust Flame* 1994, 98, 59-79.
25. Baulch, D. L.; Cobos, C. J.; Cox, R. A.; Esser, C.; Frank, P.; Just, T.; Kerr, J. A.; Pilling, M. J.; Troe, J.; Walker, R. W.; Warnatz, J. *J Phys Chem Ref Data* 1992, 21, 411.
26. Tsang, W. *J Phys Chem Ref Data* 1992, 21, 753-791.
27. Tsang, W.; Hampson, R. F. *J Phys Chem Ref Data* 1986, 15, 1087-1279.
28. Goldsmith, C. F.; Tomlin, A. S.; Klippenstein, S. J. *Proc Combust Inst* 2013, 34,

177-185.

29. Sobol', I. M.; Kucherenko, S. S. *Monte Carlo Methods and Applications* 2005, 11, 83-92.
30. Ziehn, T.; Tomlin, A. S. *Environ Model Soft* 2009, 24, 775-785.
31. Tomlin, A. S.; Ziehn, T. In *Coping with Complexity: Model Reduction and Data Analysis*; Gorban, A. N.; Roose, D., Eds.; Springer Berlin Heidelberg, 2011, p 9-36.
32. Sobol', I. M. *USSR Comput Math Math Phys* 1967, 7, 86-112.
33. Rabitz, H.; Alis, Ö. F.; Shorter, J.; Shim, K. *Comput Phys Commun* 1999, 117, 11-20.
34. Wang, S. W.; Georgopoulos, P. G.; Li, G. Y.; Rabitz, H. *J Phys Chem A* 2003, 107, 4707-4716.
35. Reagan, M. T.; Najm, H. N.; Debusschere, B. J.; Le Maitre, O. P.; Knio, O. M.; Ghanem, R. G. *Combust Theor Model* 2004, 8, 607-632.
36. Najm, H.; Debusschere, B. J.; Marzouk, Y. M.; Widmer, S.; Le Maître, O. P. *Int J Numer Meth Eng* 2009, 80, 789-814.
37. Li, G.; Rosenthal, C.; Rabitz, H. *J Phys Chem A* 2001, 105, 7765 -7777.
38. Sobol, I. M. *Math Comput Sim* 2001, 55, 271-280.
39. Rabitz, H.; Alis, O. F. In *Sensitivity Analysis*; Saltelli, A.; Chan, K.; Scott, E., Eds.; John Wiley & Sons, 2000, p 199-224.
40. Li, G. Y.; Wang, S. W.; Rabitz, H. *J Phys Chem A* 2002, 106, 8721-8733.
41. Sheen, D. A.; You, X. Q.; Wang, H.; Lovas, T. *Proc Combust Inst* 2009, 32, 535-542.
42. Dagaut, P.; Daly, C.; Simmie, J. M.; Cathonnet, M. *Proc Combust Inst* 1998, 27, 361-369.
43. Gao, J.; Nakamura, Y. *Fuel* 2013, 106, 241-248.
44. Mittal, G.; Sung, C. J.; Fairweather, M.; Tomlin, A. S.; Griffiths, J. F.; Hughes, K. J. *Proc Combust Inst* 2007, 31, 419-427.
45. Turanyi, T.; Nagy, T.; Zsely, I. G.; Cserhati, M.; Varga, T.; Szabo, B. T.; Sedyo, I.; Kiss, P. T.; Zempleni, A.; Curran, H. J. *Int J Chem Kinet* 2012, 44, 284-302.
46. Eskola, A. J.; Carr, S. A.; Shannon, R. J.; Wang, B.; Blitz, M. A. P., M.A. ; Seakins, P. W. *J Phys Chem A* 2014, submitted.
47. Andersen, A.; Carter, E. A. *Mol Phys* 2008, 106, 367-396.
48. Zador, J.; Huang, H. F.; Welz, O.; Zetterberg, J.; Osborn, D. L.; Taatjes, C. A. *Phys Chem Chem Phys* 2013, 15, 10753-10760.
49. Goldsmith, C. F.; Green, W. H.; Klippenstein, S. J. *J Phys Chem A* 2012, 116, 3325-3346.
50. Atkinson, R.; Baulch, D. L.; Cox, R. A.; Hampson, R. F.; Kerr, J. A.; Troe, J. *J Phys Chem Ref Data* 1989, 18, 881-1097.
51. Andersen, A.; Carter, E.A. *J Phys Chem A* 2003, 107, 9463-9478

## List of Figure Legends

Figure 1. Comparison between experimentally measured species profiles (black solid line) and simulated profiles for the Princeton flow reactor data<sup>11</sup>. For H<sub>2</sub>O<sub>2</sub> the grey shading represents experimental errors. The dashed line represents model simulations with unperturbed parameter values. The box and whiskers represent 25<sup>th</sup> and 75<sup>th</sup> percentiles respectively based on a quasi-random sample of 256 model runs. The large crosses represent the mean predicted output from the 256 simulations a) LLNL mechanism b) Liu2013 mechanism c) Aramco mechanism. In c) the dotted line represents the effect of isolated modifications to the rate of RO<sub>2</sub> → QOOH and QOOH → 2CH<sub>2</sub>O + OH based on the data of Eskola et al.<sup>46</sup>. The dot-dashed line represents further reduction of the forward rate of the chain-branching step QOOH+O<sub>2</sub> by a factor of 10.

Figure 2. Comparison between experimental<sup>10</sup> and simulated ignition delays a) LLNL b) Liu2013 c) Aramco. In all cases P = 10 bar.

Figure 3. Comparison between experimentally measured ignition delays (solid line) and simulated profiles for the RCM data<sup>10</sup>, φ = 0.75, 10 bar. The dashed line represents model simulations with unperturbed parameter values. The box and whiskers represent 25<sup>th</sup> and 75<sup>th</sup> percentiles respectively based on a quasi-random sample of 256 model runs. The large crosses represent the mean predicted output from the 256 simulations a) LLNL mechanism b) Liu2013 mechanism c) Aramco mechanism. In c) the dotted line represents the effect of isolated modifications to the rate of RO<sub>2</sub> → QOOH and QOOH → 2CH<sub>2</sub>O + OH based on the data of Eskola et al.<sup>46</sup>. The dot-dashed line represents further modification of the forward rate of the chain-branching step QOOH+O<sub>2</sub> by a factor of 5.

Figure 4. Main sensitivity indices (first- and second-order) for simulated flow reactor simulations with respect to reaction rates at selected temperatures. A comparison between each mechanism is given and shading for each reaction or pair of reactions is shown in the legend. a) CH<sub>2</sub>O mole fraction b) CH<sub>3</sub>OCHO mole fraction c) H<sub>2</sub>O<sub>2</sub> mole fraction d) legend.

Figure 5 Main pathways which dominate the uncertainty in predicted species mole fractions for CH<sub>2</sub>O, CH<sub>3</sub>OCHO, H<sub>2</sub>O<sub>2</sub> and ignition delays.

Figure 6. First-order HDMR component functions (solid line) of simulated mole fractions shown on-top of the scatter resulting from the quasi-random sampling for a) 550 K, sensitivity of CH<sub>2</sub>O to changes in forward rate of RO<sub>2</sub> = QOOH b) 550 K, sensitivity of CH<sub>3</sub>OCHO to changes in forward rate of RO<sub>2</sub> = QOOH. The Aramco mechanism is used in each case and 2000 data points are shown.

Figure 7. First-order HDMR component functions (solid line) of simulated mole fractions shown on-top of the scatter resulting from the quasi-random sampling for a) 650K, sensitivity of CH<sub>3</sub>OCHO to changes in forward rate of RO<sub>2</sub> = QOOH b) 650K, sensitivity of H<sub>2</sub>O<sub>2</sub> to changes in forward rate of RO<sub>2</sub> = QOOH c) 650K sensitivity of CH<sub>2</sub>O to forward rate for QOOH + O<sub>2</sub> d) 700K sensitivity of CH<sub>2</sub>O to forward rate for QOOH + O<sub>2</sub>. The Aramco mechanism is used in each case and 2000 data points are shown.

Figure 8. Main sensitivity indices (first- and second-order) for simulated ignition delays with respect to reaction rates at selected temperatures and pressures. A comparison between each mechanism is given and shading for each reaction or pair of reactions is shown in the legend a) sensitivity coefficients b) legend.

Figure 9. HDMR component functions (solid line) of simulated ignition delays shown on-top of the scatter resulting from the quasi-random sampling in the case of first-order functions. P = 10 bar, φ = 0.75, T = 703 K. Sensitivity with respect to a) forward rate of RO<sub>2</sub> = QOOH b) forward rate of QOOH + O<sub>2</sub> c) forward rate of QOOH = 2CH<sub>2</sub>O + OH d) second-order component function representing the interactive effect of forward rates for QOOH + O<sub>2</sub> and QOOH = 2CH<sub>2</sub>O + OH.

Figure 10. A comparison of current data within the LLNL, LIU2013 and Aramco mechanisms compared to new data from a recent study of Eskola et al.<sup>46</sup> a) RO<sub>2</sub> → QOOH b) QOOH → 2CH<sub>2</sub>O + OH.

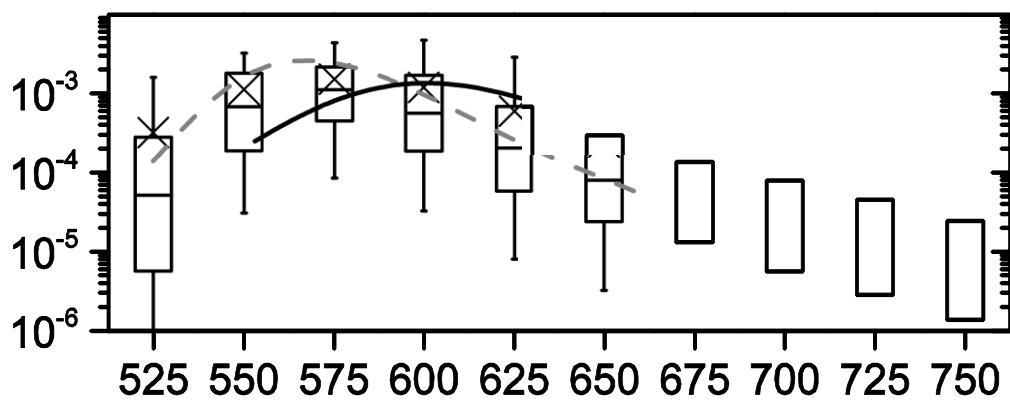


Table 1. Reactions selected from linear screening analysis and assigned input uncertainty factors.

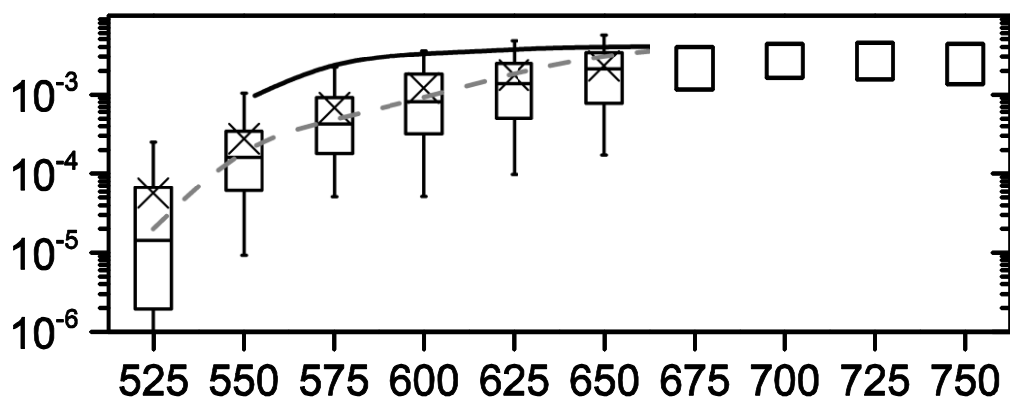
Reaction	$G_i$	Screened for flow reactor	Screened for RCM	Source of uncertainty information
$H + O_2 (+ M) = HO_2 (+ M) (k_c)$	3.16	*	x	<sup>23</sup>
$H + O_2 (+ M) = HO_2 (+ M) (k_0)$	1.58	*	x	<sup>23</sup>
$H + O_2 = O + OH$	1.41		x	<sup>23</sup>
$OH^* + O_2 = OH + O_2$	10.00		x	Estimated
$HO_2 + H = OH + OH$	1.41	*	x	<sup>23</sup>
$HO_2 + HO_2 = H_2O_2 + O_2$	1.41	*	x	<sup>23</sup>
$HO_2 + OH = H_2O + O_2$	3.16		x	<sup>23</sup>
$H_2O_2 + H = H_2O + OH$	2.00	*	x	<sup>26</sup>
$H_2O_2 + OH = H_2O + HO_2$	1.58	*	x	<sup>26</sup>
$H_2O_2 (+ M) = OH + OH (+M) (k_0, k_c)$	3.16		x	<sup>23</sup>
$HCO + O_2 = O_2CHO$	10.0	*	x	Estimated
$HCO + O_2 = CO + HO_2$	2.24	*	x	<sup>23</sup>
$CH_2O + OH = HCO + H_2O$	2.24	*	x	<sup>23</sup>
$CH_2O + H = HCO + H_2$	1.58	*		<sup>23</sup>
$CH_2O + HO_2 = HCO + H_2O_2$	2.00	*	x	<sup>23</sup>
$CH_2O + OH = HOCH_2O$	10.0	*		Estimated
$OCHO + HO_2 = HOCHO + O_2$	10.0	*		Estimated
$CH_3 + HO_2 = OH + CH_3O$	10.0		x	<sup>23</sup>
$CH_3 + HO_2 = CH_4 + O_2$	10.0		x	Estimated
$CH_3 + CH_3 (+ M) = C_2H_6 (+ M) (k_0, k_c)$	2.00		x	<sup>23</sup>
$CH_4 + H = CH_3 + H_2$	2.82		x	<sup>23</sup>
$HOCHO + OH = H_2O + CO_2 + H$	1.58	*	x	<sup>50</sup>
$HOCHO + H = H_2 + CO + OH$	10.0	*	x	Estimated
$HOCHO + HO_2 = H_2O_2 + CO + OH$	10.0		x	Estimated
$HOCH_2O = HCOOH + H$	10.0	*		Estimated
$HOCH_2O = HOCHO + H$	10.0		x	Estimated
$HCOOH + HO_2 = H_2O_2 + CO + OH$	10.0	*	x	Estimated
$HCOOH + OH = H_2O + CO_2 + H$	10.0		x	Estimated
$CH_3OCH_3 + OH = H_2O + CH_3OCH_2$	2.24	*	x	<sup>23</sup>
$CH_3OCH_3 + H = H_2 + CH_3OCH_2$	3.16	*	x	<sup>23</sup>
$CH_3OCH_2 = CH_2O + CH_3$	2.00		x	Estimated
$CH_3OCH_3 + HO_2 = CH_3OCH_2 + H_2O_2$	10.0	*	x	Estimated
$CH_3OCH_3 + O_2 = CH_3OCH_2 + HO_2$	5.00		x	<sup>23</sup>
$CH_3OCH_3 + CH_3OCH_2O_2 = CH_3OCH_2 + CH_3OCH_2O_2H$	10.0	*	x	Estimated
$CH_3OCH_2 + HO_2 = CH_3OCH_2O + OH$	10.0	*		Estimated
$CH_3OCH_2O_2 + CH_2O = CH_3OCH_2O_2H + HCO$	10.0	*	x	Estimated
$CH_3OCH_2O_2 + CH_3OCH_2O_2 = O_2 + 2CH_3OCH_2O$	7.94	*	x	Estimated
$CH_3OCH_2O_2 + CH_3OCH_2O_2 = O_2 + CH_3OCHO + CH_3OCH_2OH$	10.0	*	x	Estimated
$CH_3OCH_2O_2 = CH_2OCH_2O_2H$	10.0	*	x	Estimated
$CH_2OCH_2O_2H = OH + 2CH_2O$	5.00	*	x	Estimated
$CH_2OCH_2O_2H + O_2 = O_2CH_2OCH_2O_2H$	10.0	*	x	Estimated
$O_2CH_2OCH_2O_2H = HO_2CH_2OCHO + OH$	10.0		x	Estimated
$HO_2CH_2OCHO = OCH_2OCHO + OH$	10.0	*	x	Estimated
$OCH_2OCHO = CH_2O + OCHO$	10.0	*	x	Estimated
$OCH_2OCHO = HOCH_2OCO$	10.0	*	x	Estimated
$CH_3 + OCHO = CH_3OCHO$	10.0	*	x	Estimated
$CH_3OCHO + OH = CH_3OCO + H_2O$	5.00	*	x	Estimated
$CH_3OCHO + OH = CH_2OCHO + H_2O$	5.00	*	x	Estimated
$HOCH_2O + CO = HOCH_2OCO$	10.0	*	x	Estimated
$CH_2OH + CO_2 = HOCH_2OCO$	10.0	*	x	Estimated



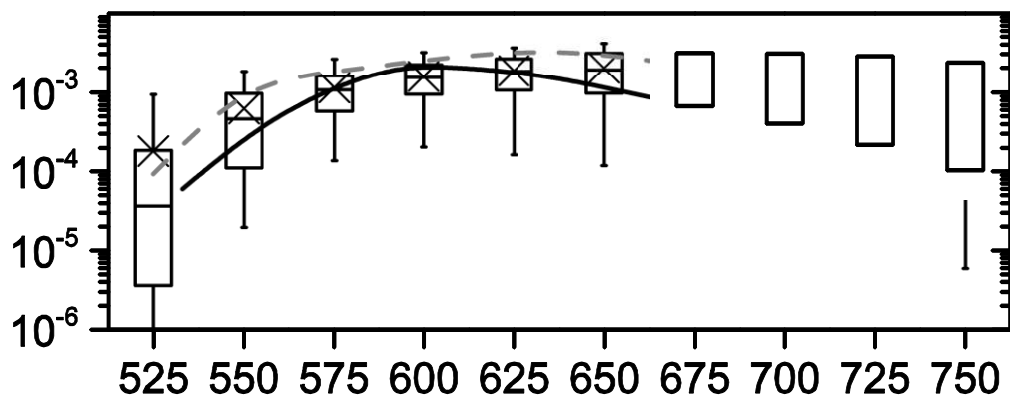
CH<sub>3</sub>OCHO mole fraction [-]



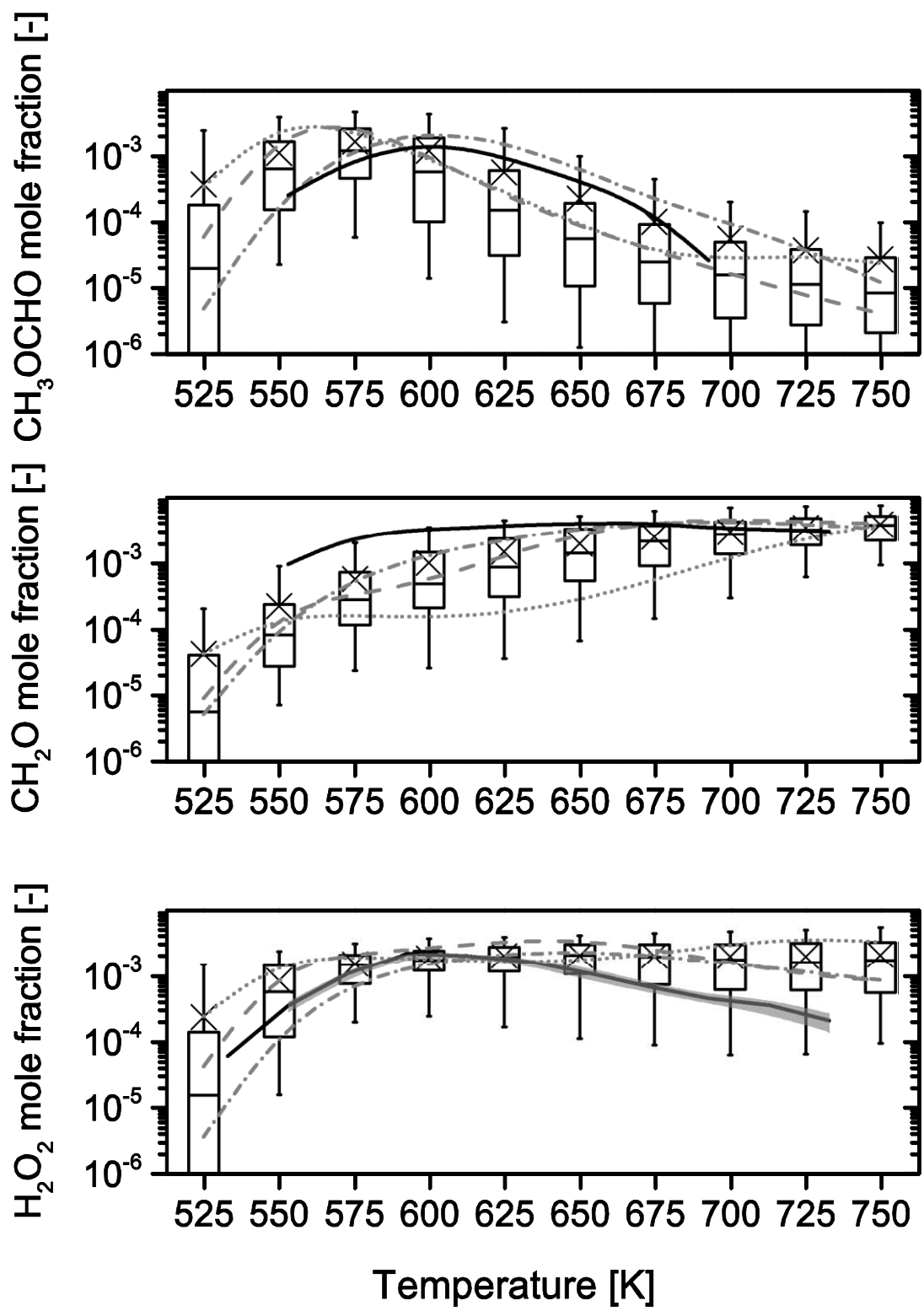
CH<sub>2</sub>O mole fraction [-]



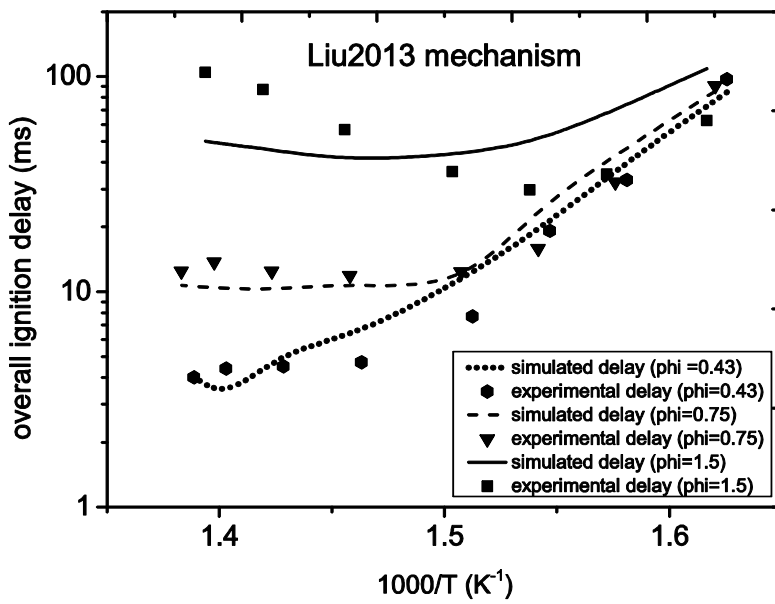
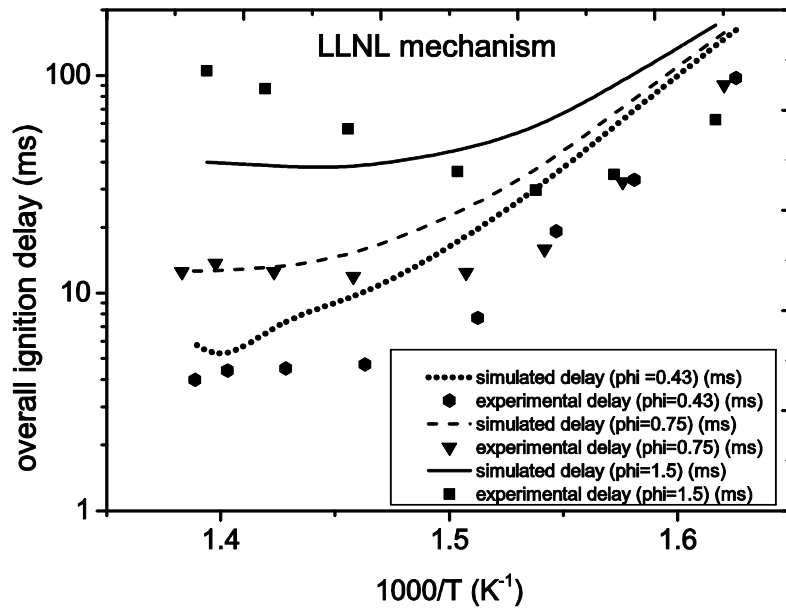
H<sub>2</sub>O<sub>2</sub> mole fraction [-]



Temperature [K]



Fig



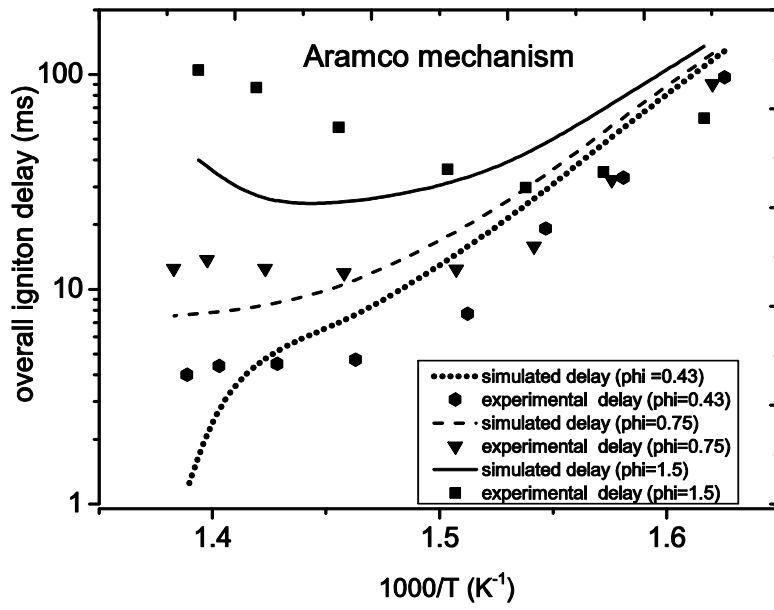
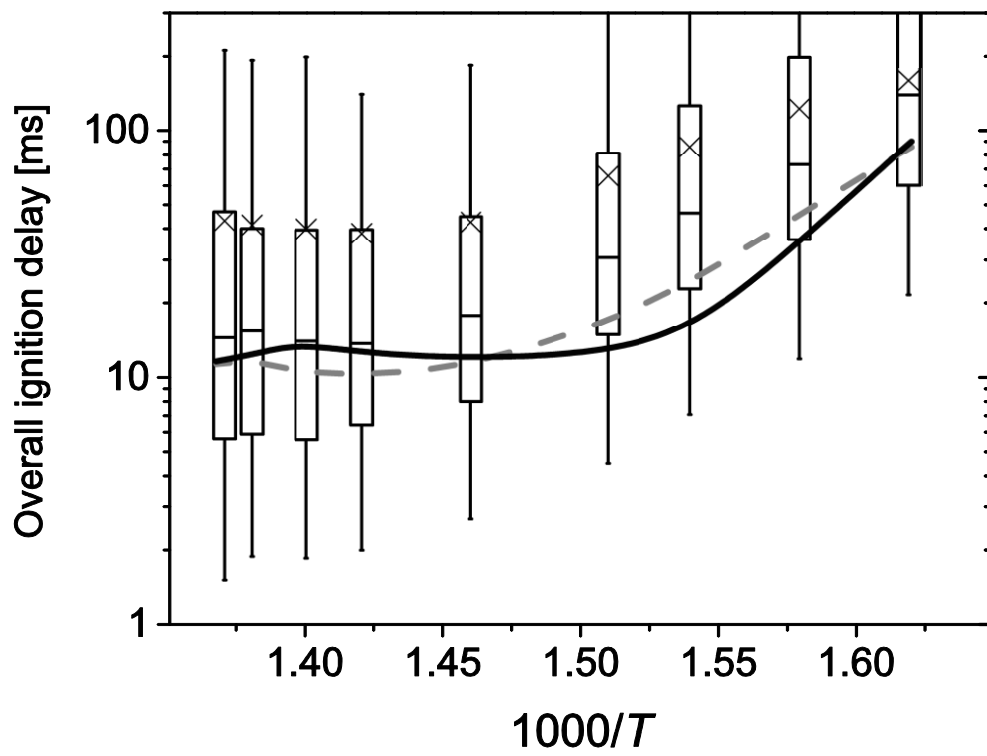
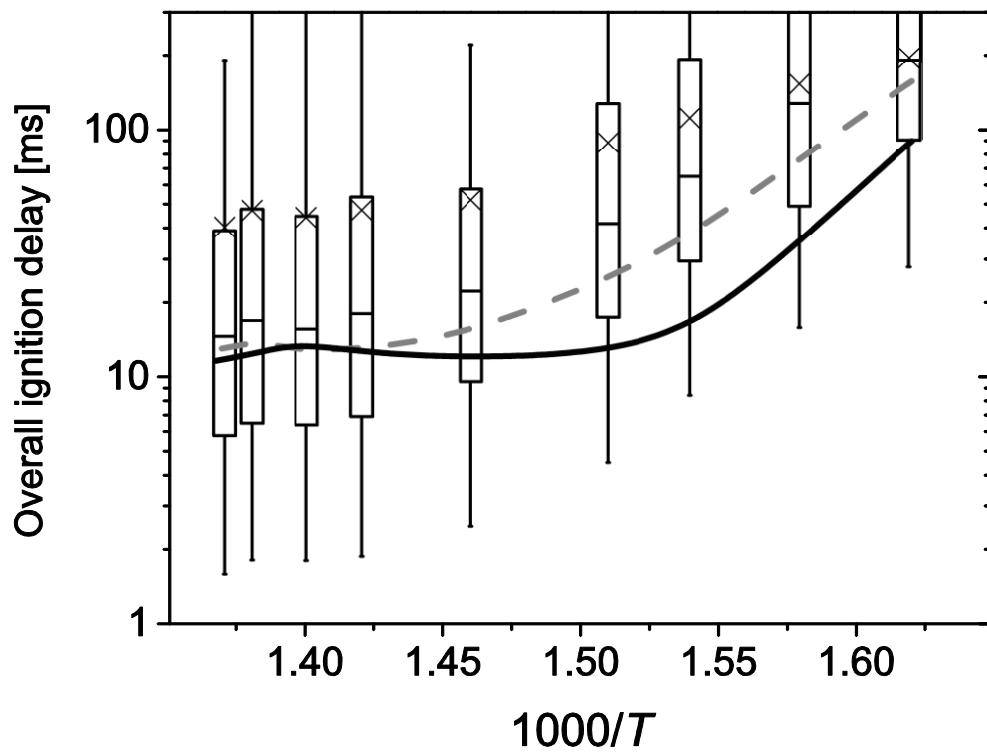
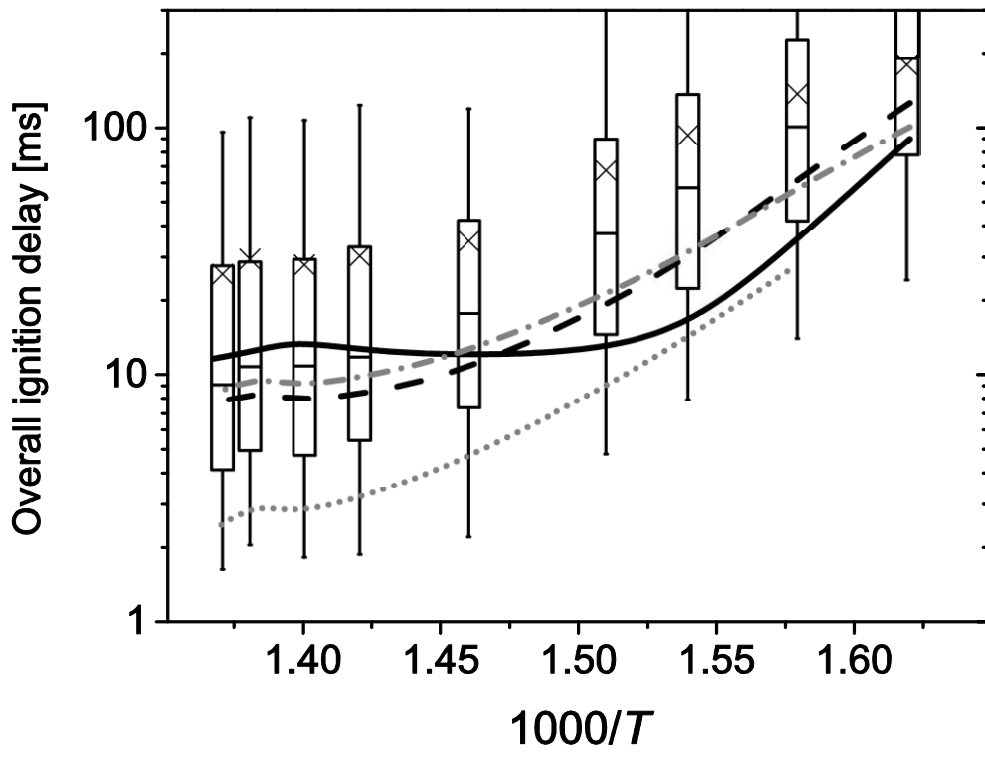


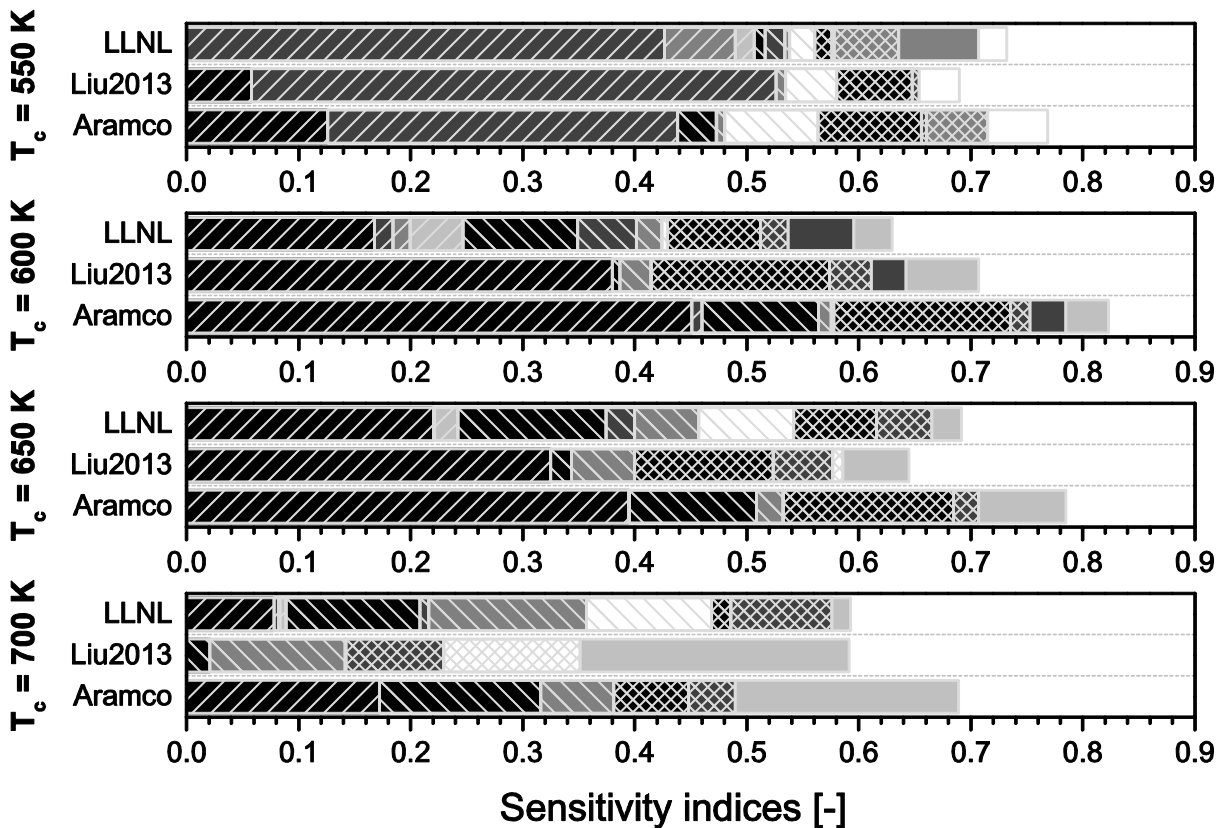
Fig 2





Fig

- $S_{i,j}: RO_2=QOOH:RO_2+RO_2$
- $S_{i,j}: QOOH=OH+2CH_2O:O_2+QOOH$
- $S_{i,j}: QOOH=>RO_2:O_2+QOOH$
- $S_{i,j}: RO_2=QOOH:O_2+QOOH$
- $S_{i,j}: QOOH=>RO_2:RO_2=>QOOH$
- $CH_3OCH_3+HO_2=CH_3OCH_2+H_2O_2$
- $H+O_2(+M)=HO_2(+M)$
- $HO_2CH_2OCHO=OCH_2OCHO+OH$
- $CH_2O+OH=HCO+H_2O$
- $CH_2OCH_2O_2H=OH+2CH_2O$
- $CH_3OCH_2O_2+CH_3OCH_2O_2=O_2+2CH_3OCH_2O$
- $CH_3OCH_2O_2+CH_3OCH_2O_2=O_2+CH_3OCHO+CH_3OCH_2OH$
- $CH_3OCH_3+OH=CH_3OCH_2+H_2O$
- $OCH_2OCHO=HOCH_2OCO$
- $CH_2O+OH=HOCH_2O$
- $CH_3OCH_2O_2+CH_2O=CH_3OCH_2O_2H+HCO$
- $OCH_2OCHO=CH_2O+OCHO$
- $CH_2OCH_2O_2H=>CH_3OCH_2O_2$
- $CH_3OCH_2O_2=CH_2OCH_2O_2H$
- $CH_2OCH_2O_2H+O_2=O_2CH_2OCH_2O_2H$



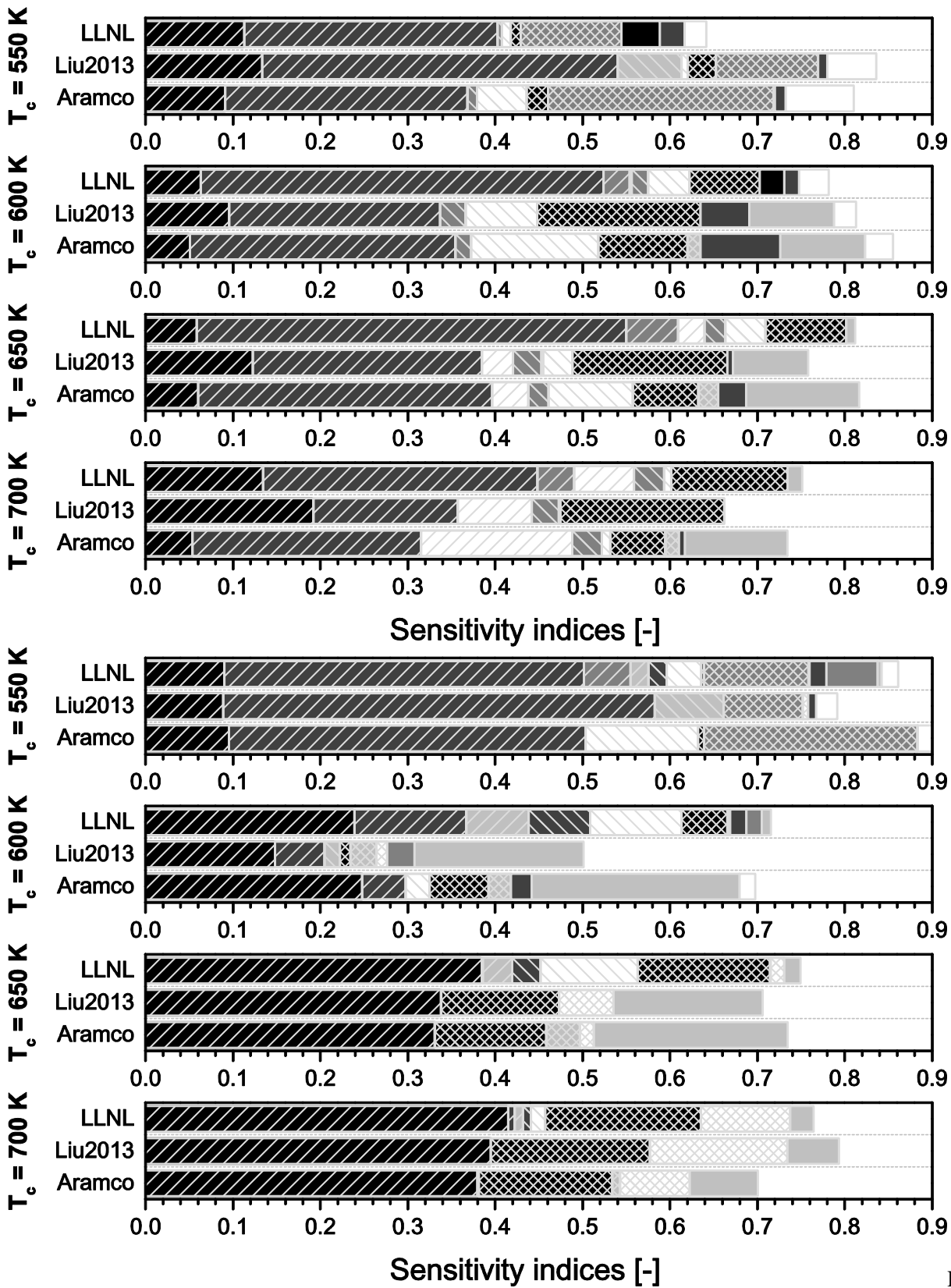


Fig4

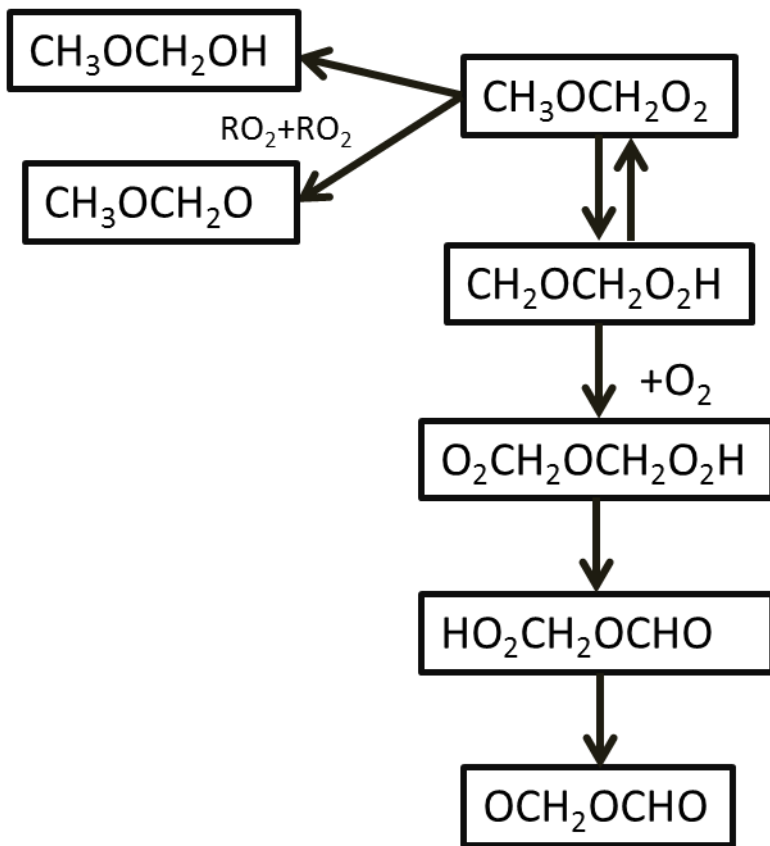
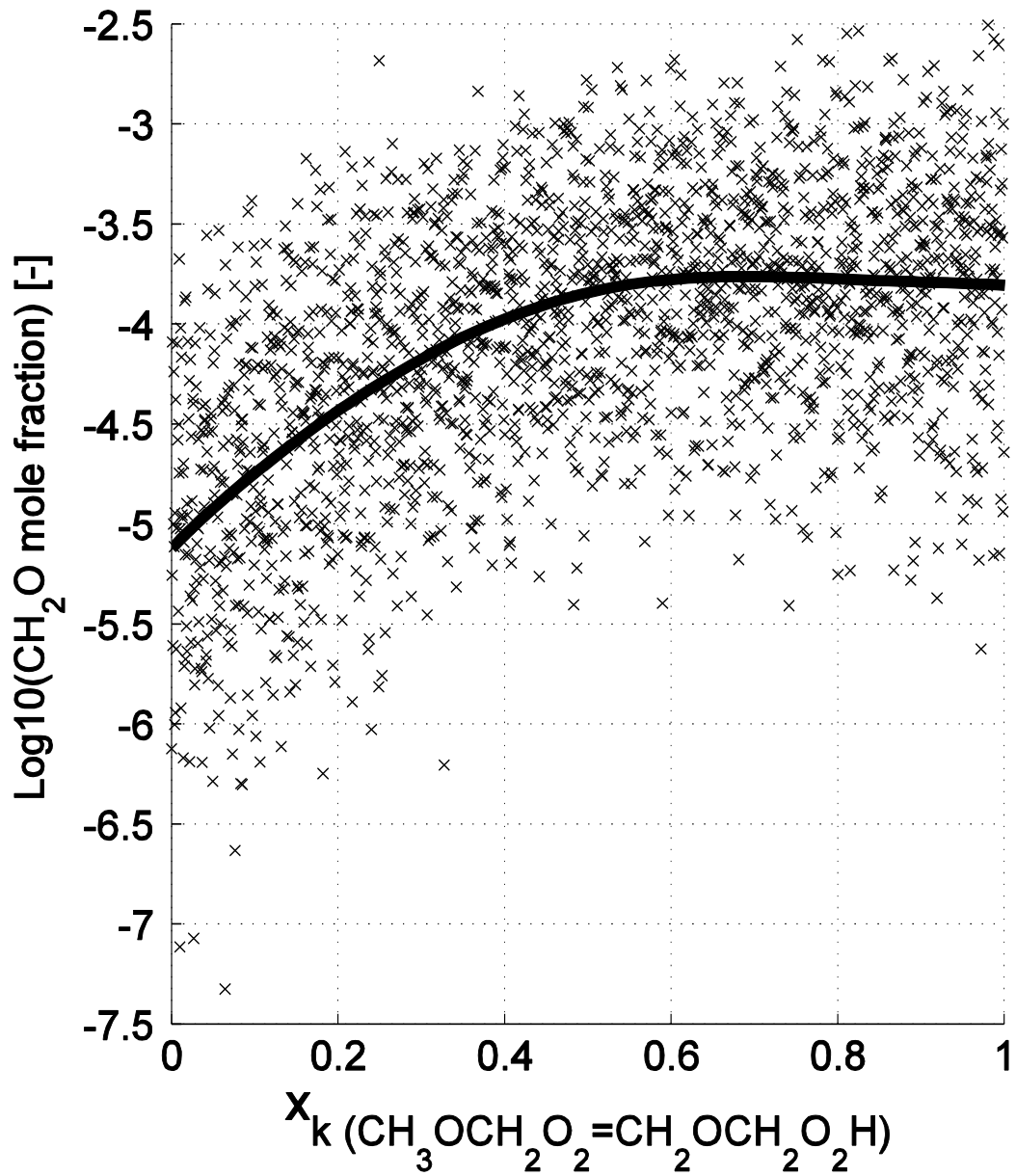
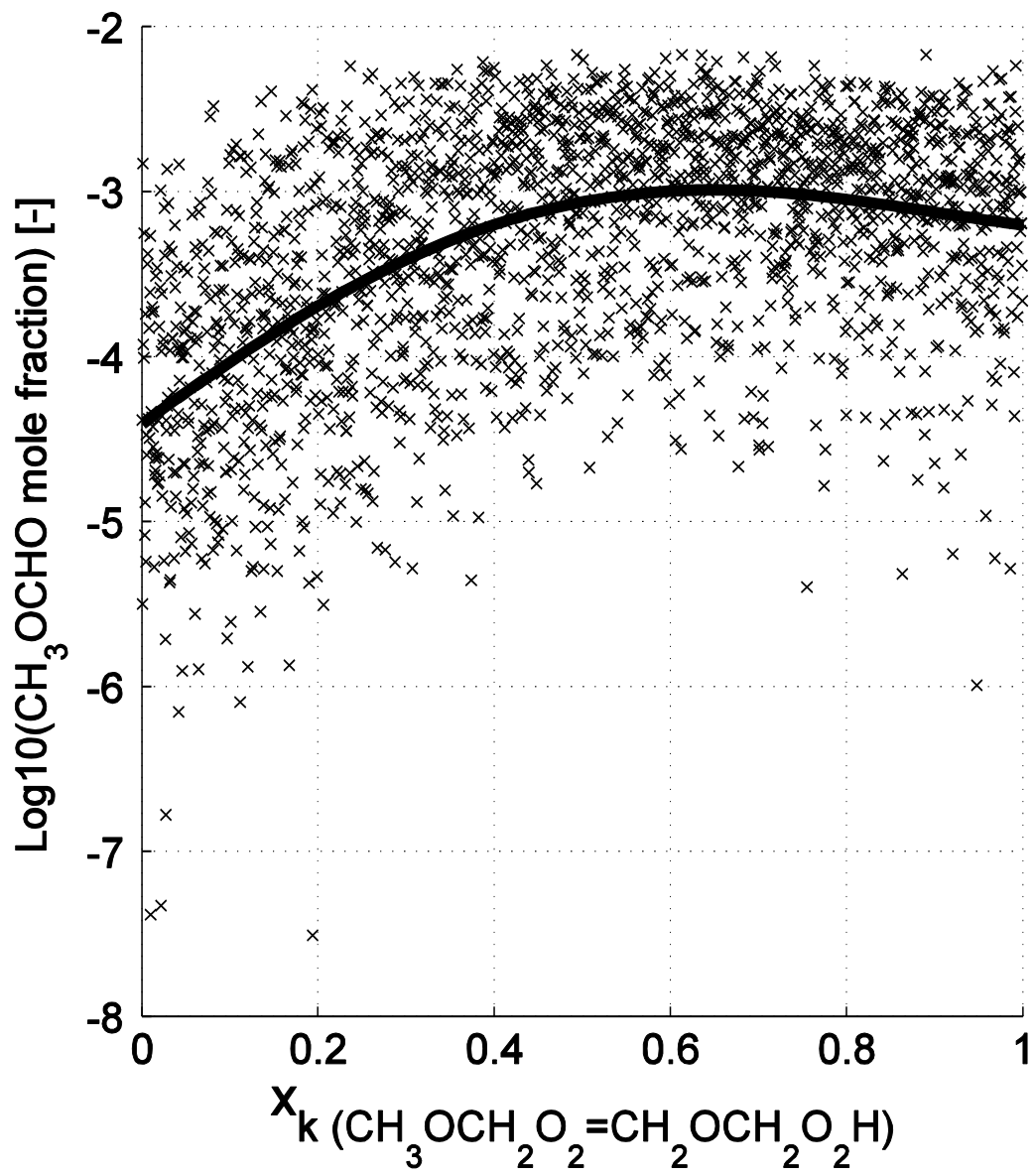
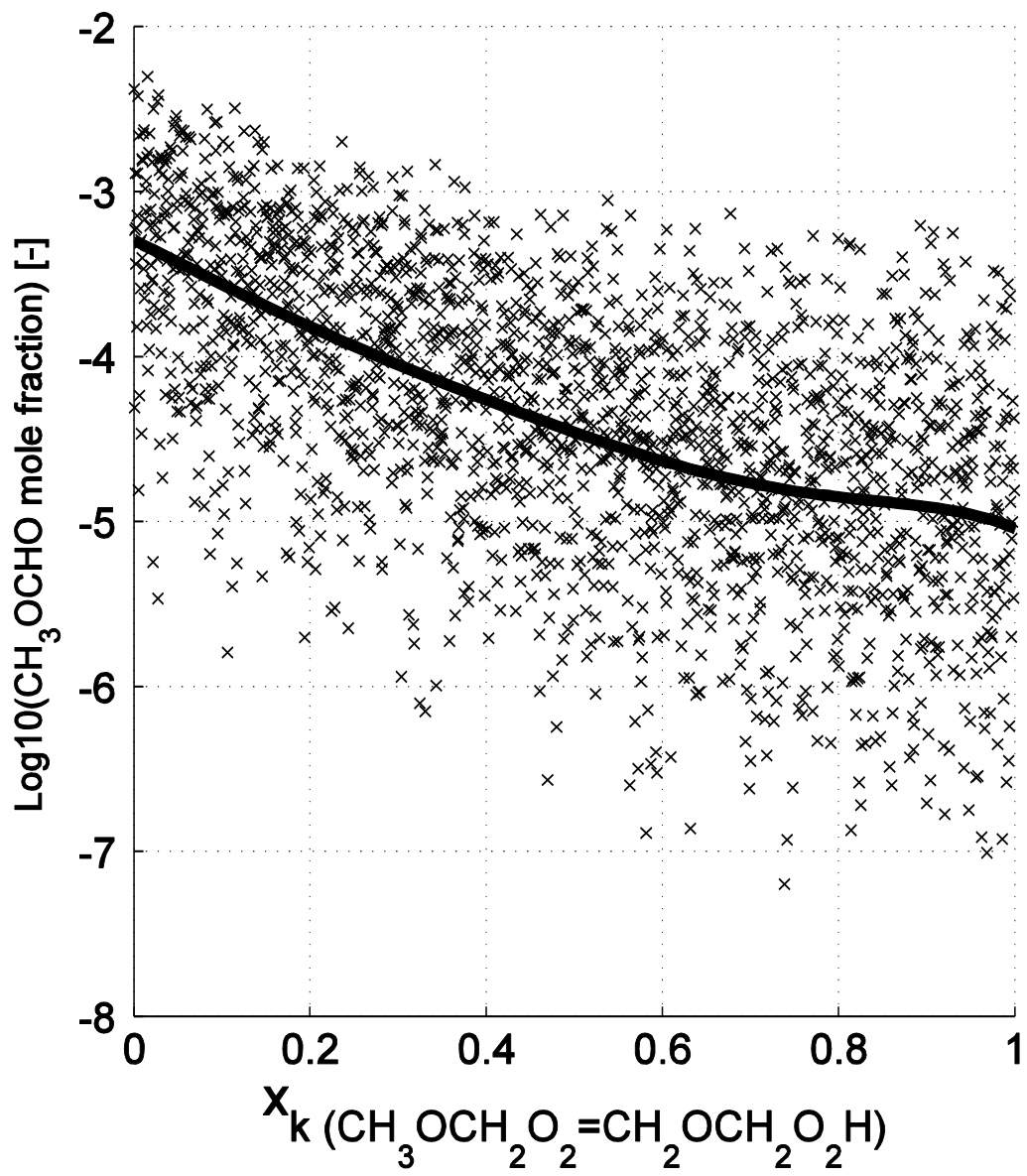


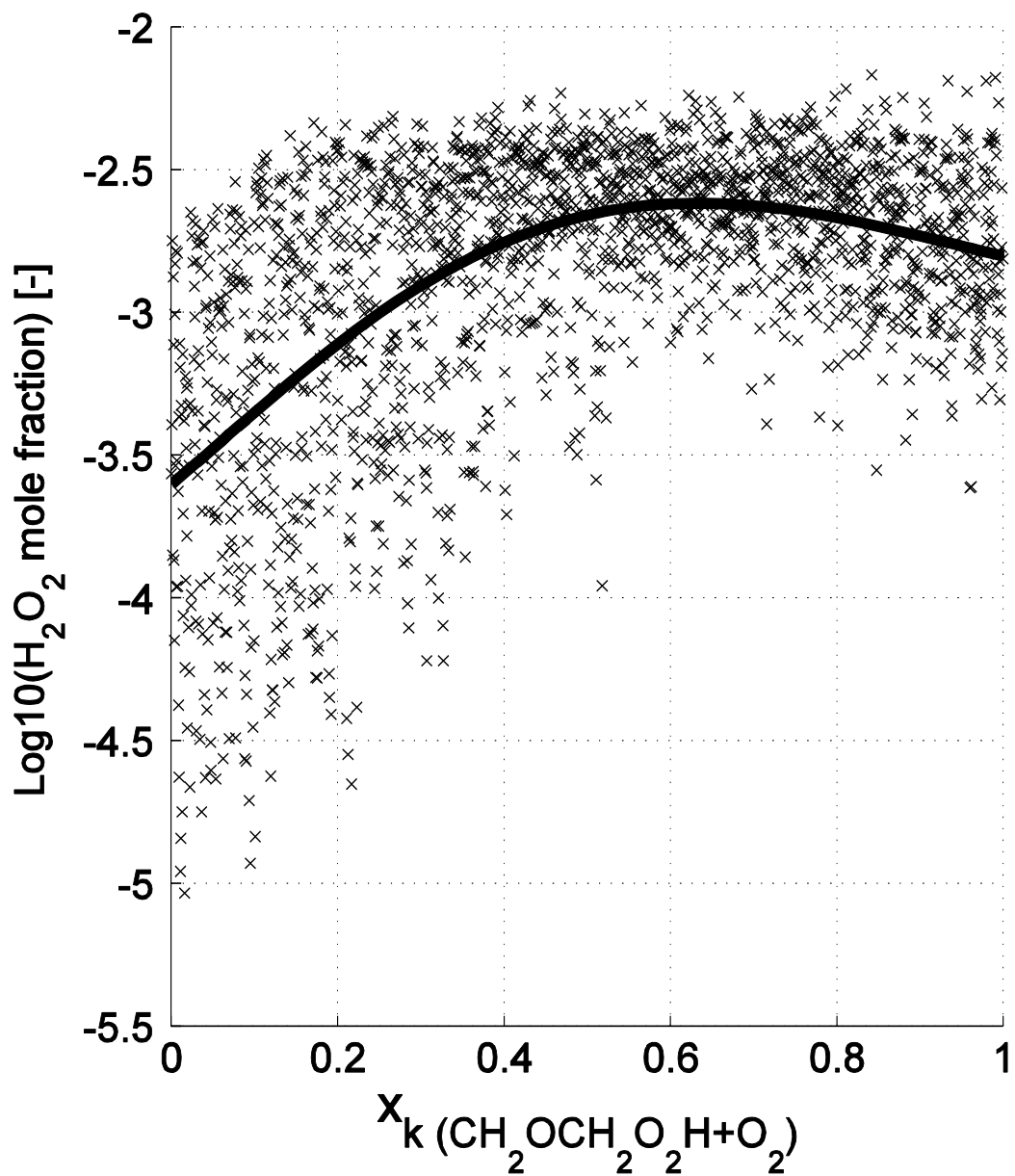
Fig 5

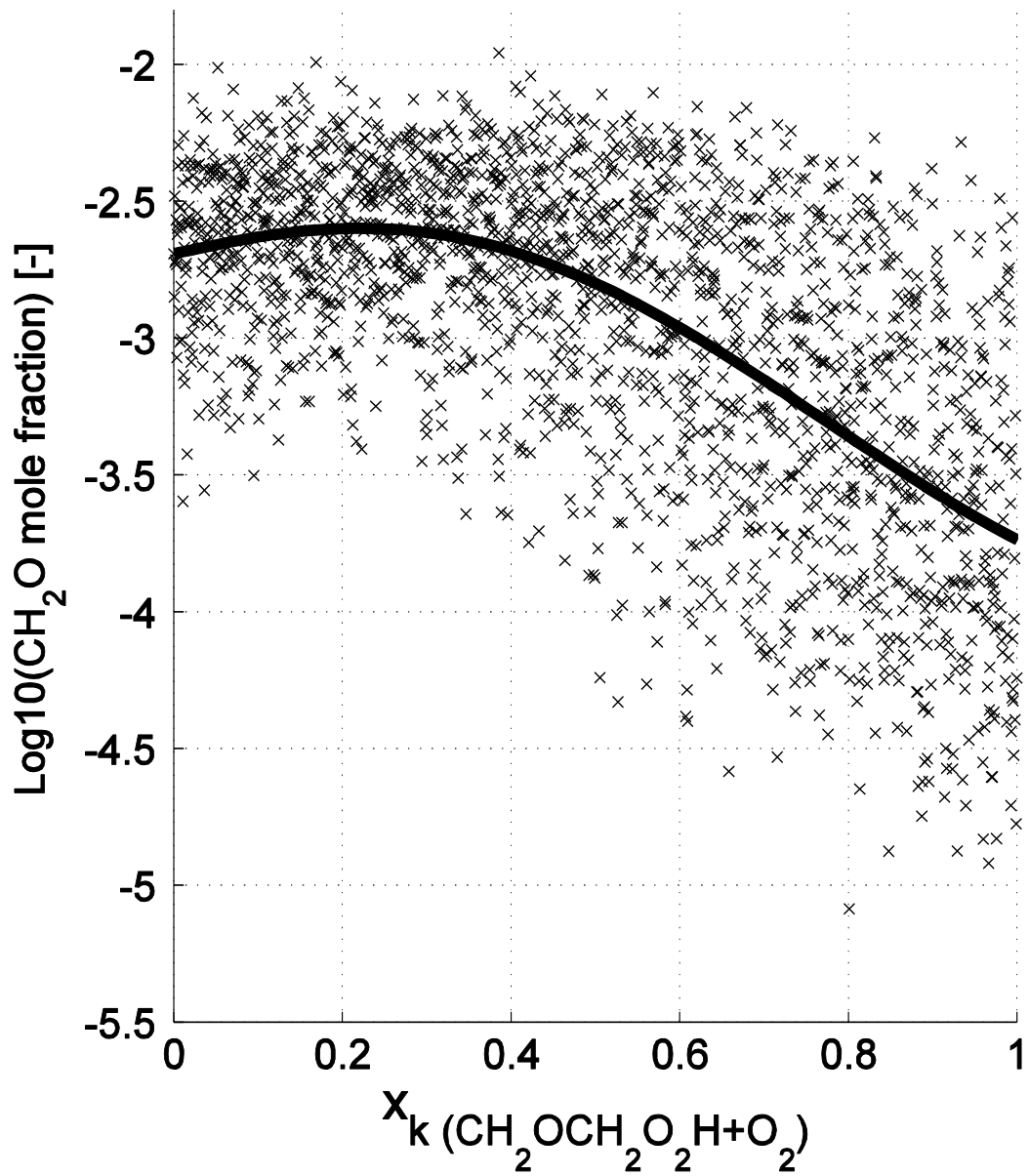


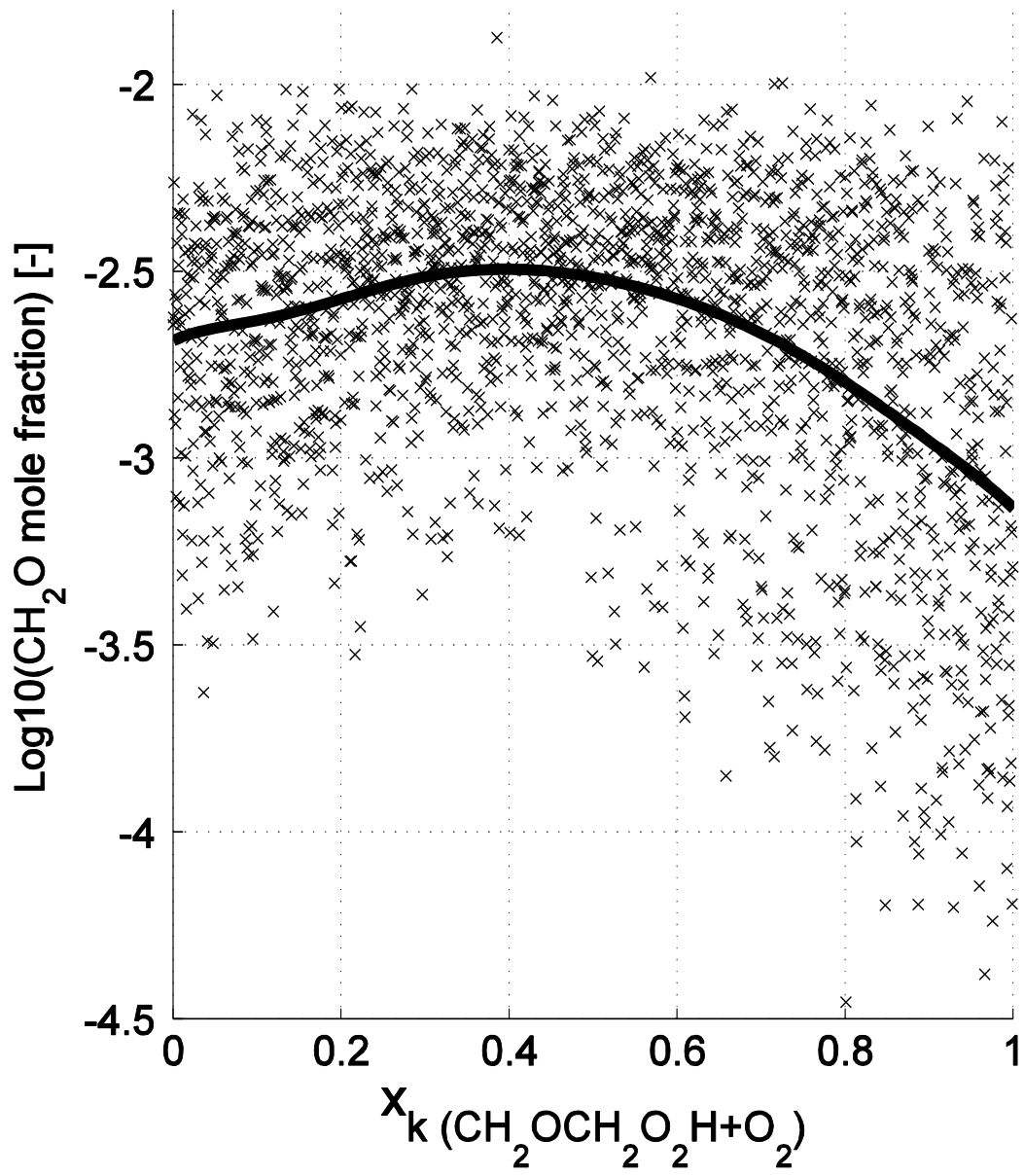


Fig



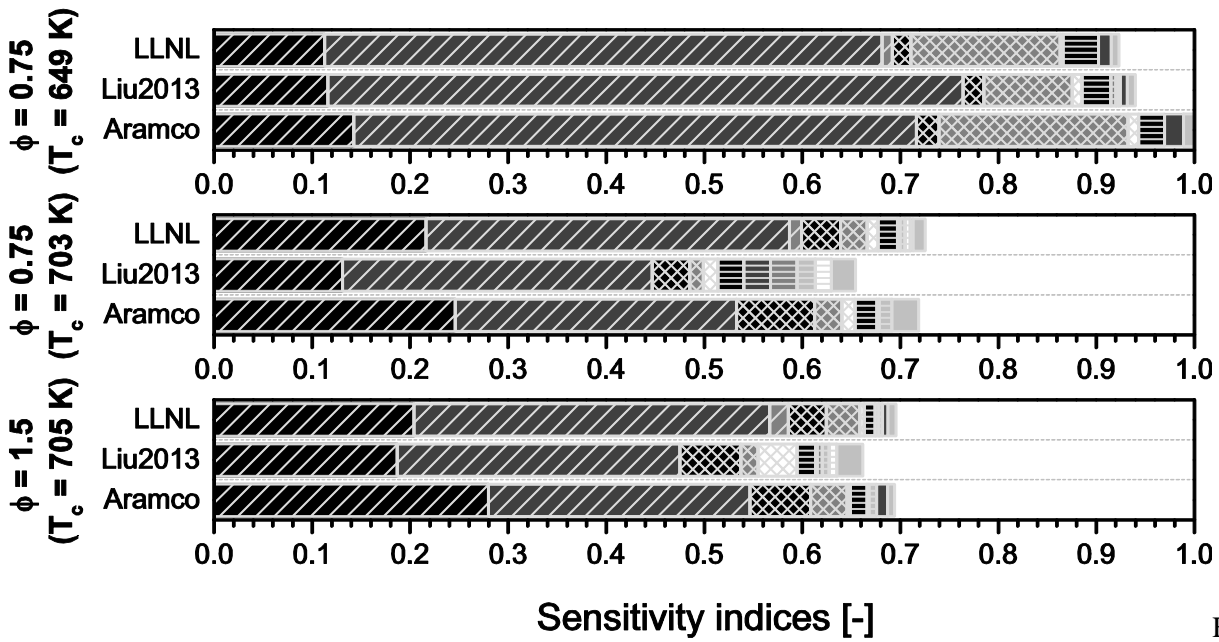




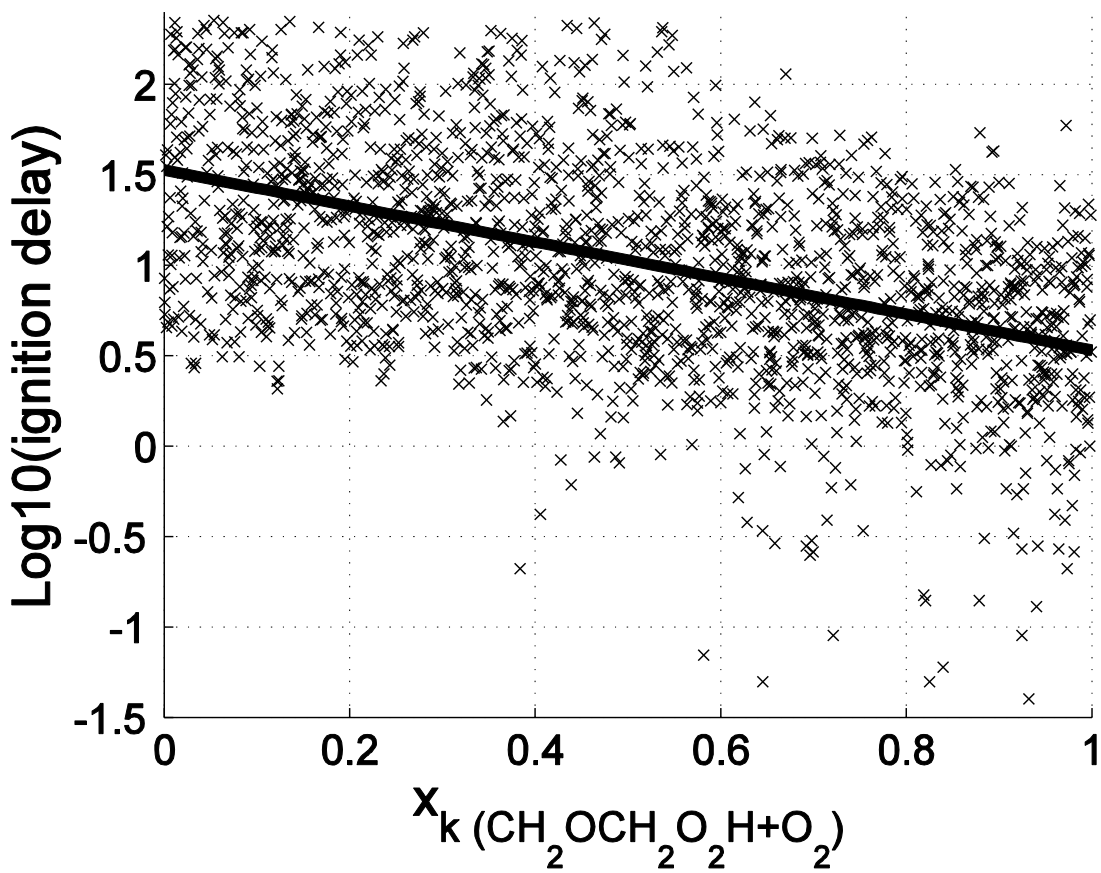
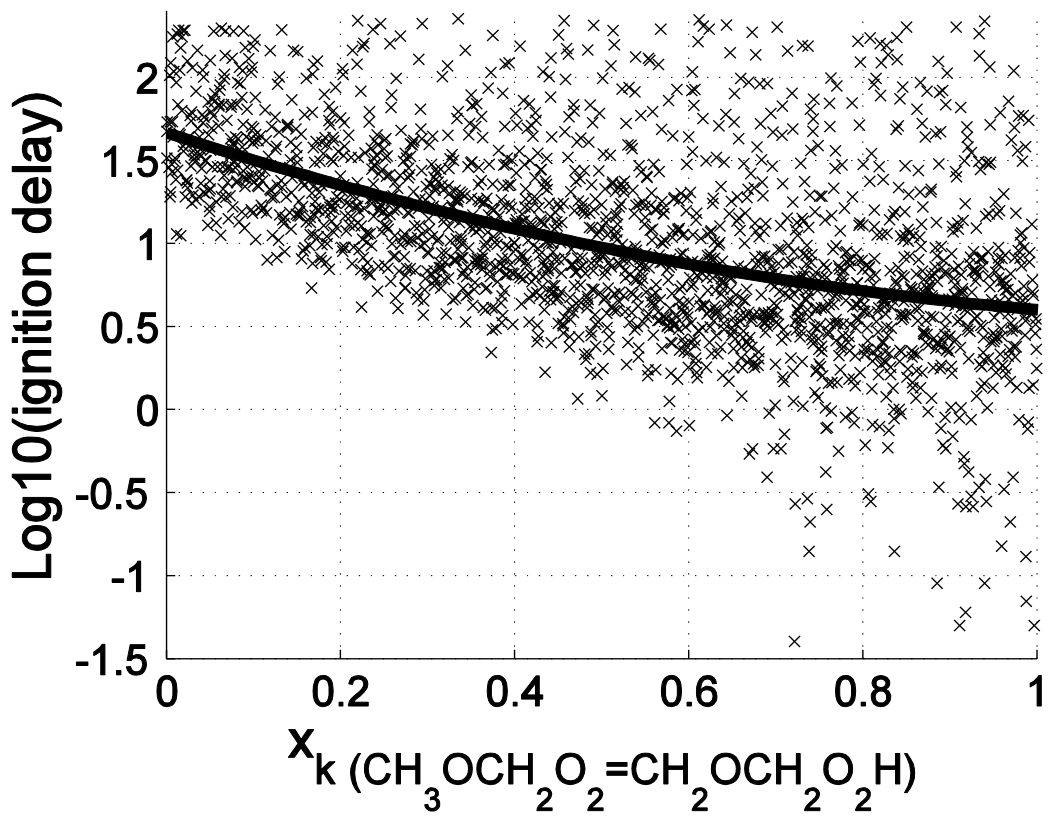


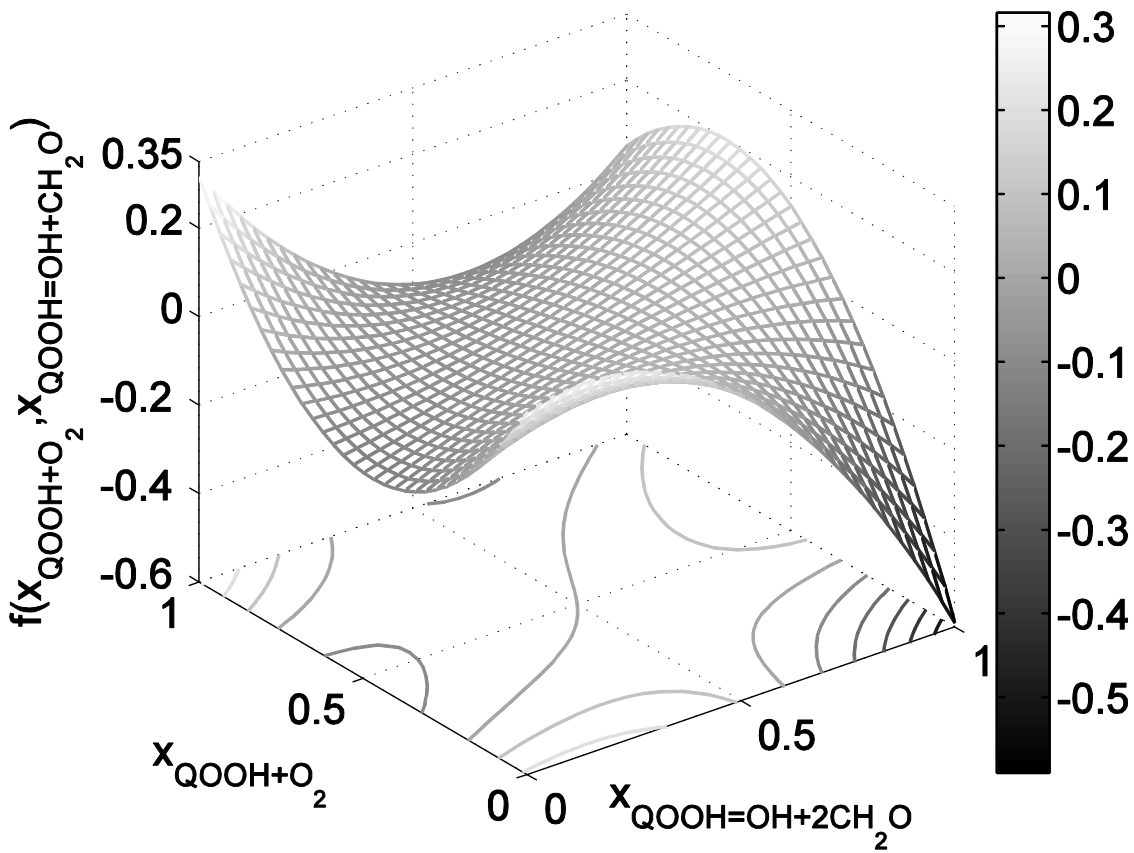
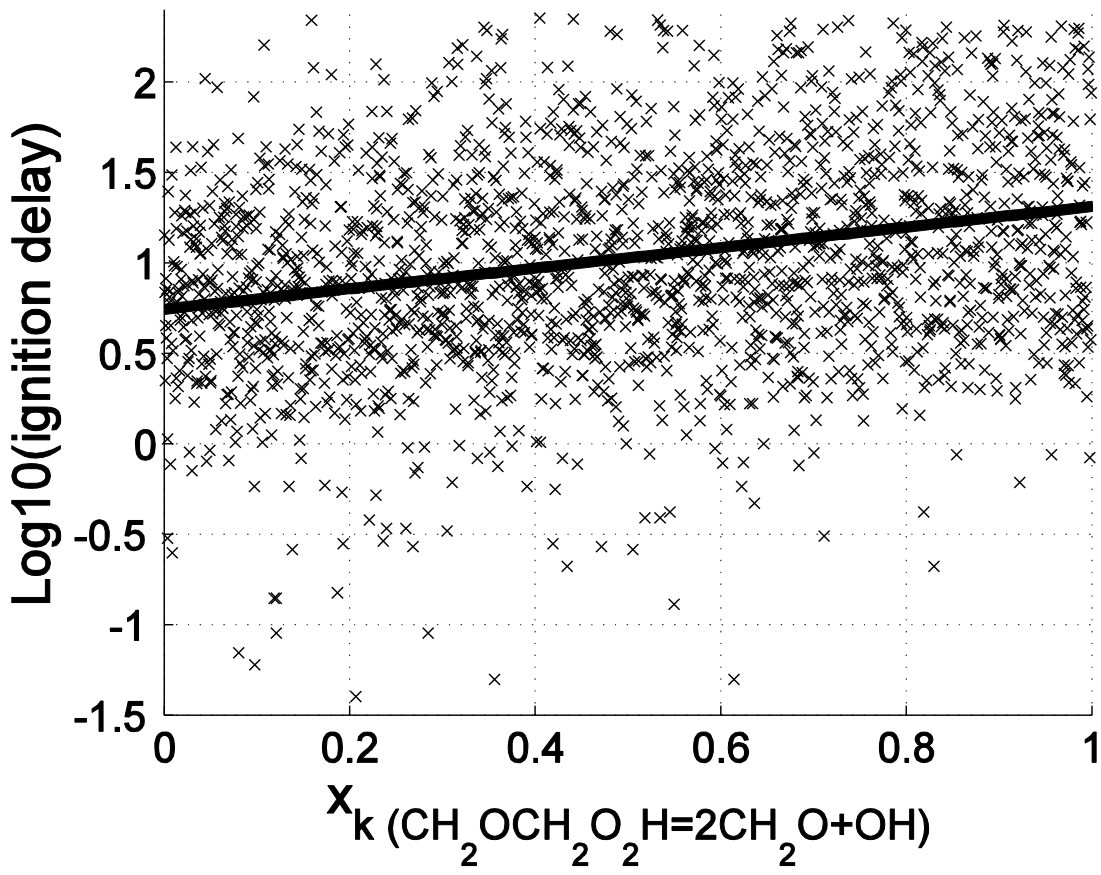
Fig

- $S_{i,j}$ :  $\text{QOOH}=\text{OH}+2\text{CH}_2\text{O}:\text{O}_2+\text{QOOH}$
- $S_{i,j}$ :  $\text{RO}_2=\text{QOOH}:\text{O}_2+\text{QOOH}$
- $S_{i,j}$ :  $\text{CH}_3\text{OCH}_3+\text{HO}_2:\text{QOOH}=\text{OH}+2\text{CH}_2\text{O}$
- $S_{i,j}$ :  $\text{CH}_3\text{OCH}_3+\text{HO}_2:\text{QOOH}+\text{O}_2$
- $\text{CH}_3+\text{HO}_2=\text{CH}_4+\text{O}_2$
- $\text{CH}_3+\text{HO}_2=\text{OH}+\text{CH}_3\text{O}$
- $\text{O}_2\text{CH}_2\text{OCH}_2\text{O}_2\text{H}=\text{HO}_2\text{CH}_2\text{OCHO}+\text{OH}$
- $\text{CH}_3\text{OCH}_3+\text{HO}_2=\text{CH}_3\text{OCH}_2+\text{H}_2\text{O}_2$
- $\text{HO}_2\text{CH}_2\text{OCHO}=\text{OCH}_2\text{OCHO}+\text{OH}$
- $\text{CH}_2\text{OCH}_2\text{O}_2\text{H}=\text{OH}+2\text{CH}_2\text{O}$
- $\text{CH}_2\text{OCH}_2\text{O}_2\text{H}=\text{CH}_3\text{OCH}_2\text{O}_2$
- $\text{CH}_3\text{OCH}_2\text{O}_2=\text{CH}_2\text{OCH}_2\text{O}_2\text{H}$
- $\text{CH}_2\text{OCH}_2\text{O}_2\text{H}+\text{O}_2=\text{O}_2\text{CH}_2\text{OCH}_2\text{O}_2\text{H}$



Fig





Fig

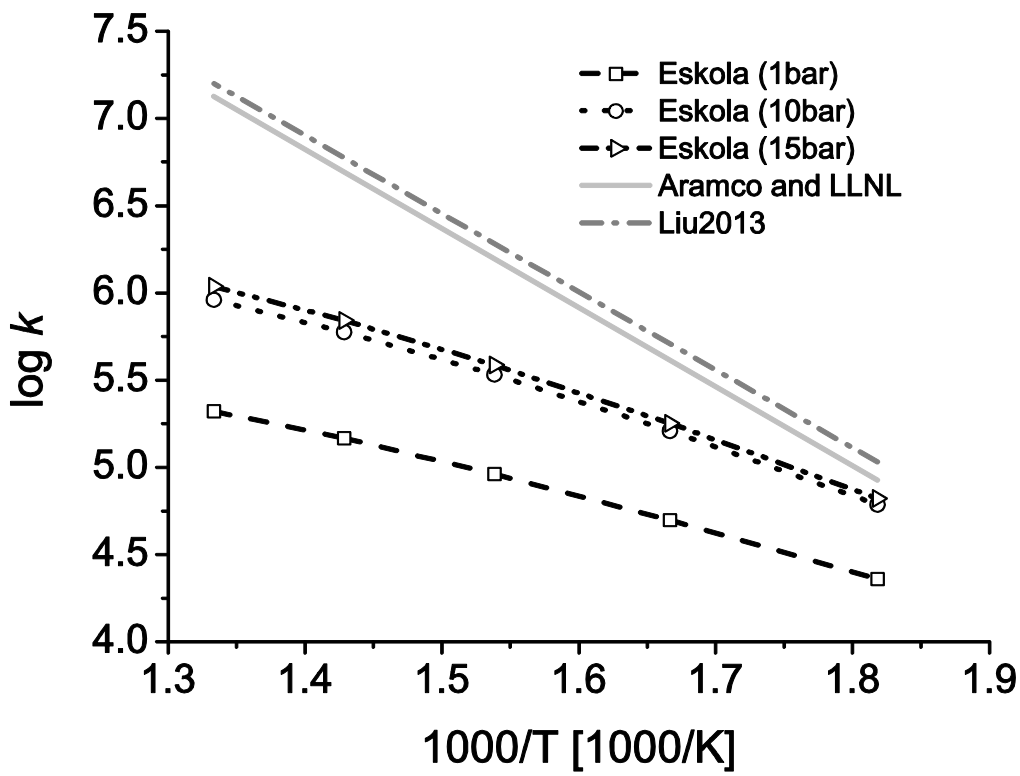
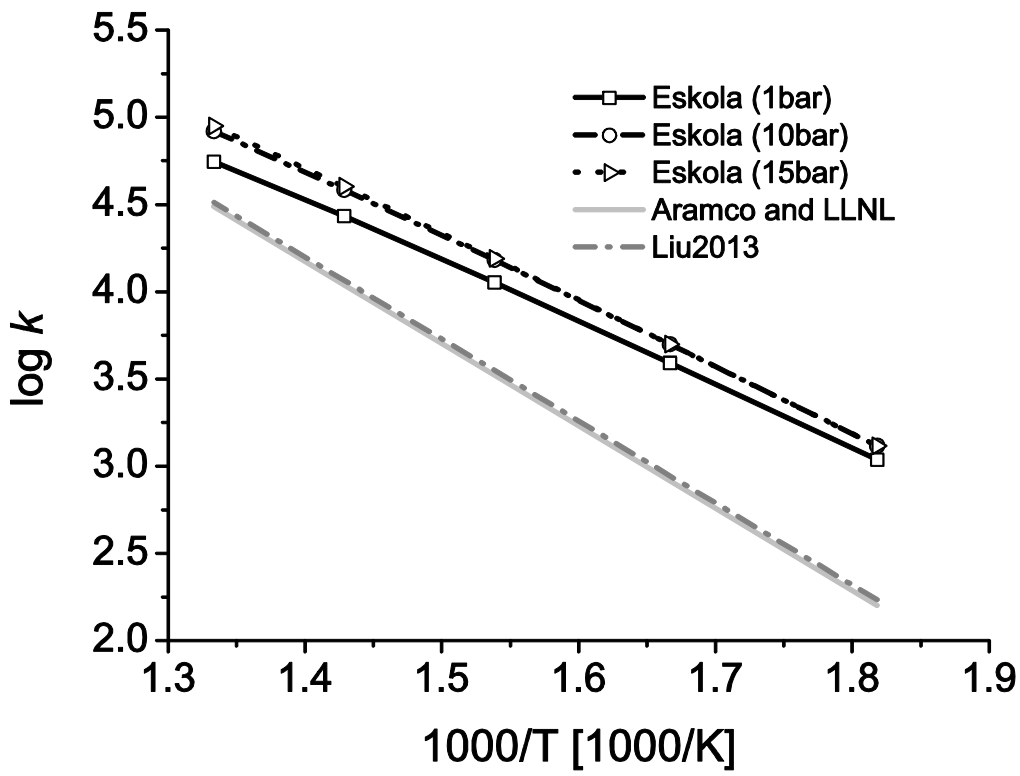


Fig 10